9
Two-dimensional fields of limiting stress

9.1 Coulomb's Analysis of Active Pressure using a Plane Surface of Slip

In 1776, before the concept of stress was clear, Coulomb[1] published his notable first paper on the application of the differential calculus to problems of architectural statics. His basic assumption was that the effective stress components σ' normal and τ tangential to a rupture plane satisfied a relationship such as

$$|\tau| \leq k + \sigma' \tan\rho. \qquad \text{(8.1 bis)}$$

But the importance of Coulomb's work lies in the analysis that he developed rather than in this basic assumption.

Let us consider the simple case of a smooth vertical wall which retains a horizontal layer of uniform soil, illustrated by the section of Fig. 9.1(a). For convenience, the analysis will be applied to unit length of the wall (perpendicular to the section) and we shall examine the conditions of limiting equilibrium which apply to one possible (plane) surface of rupture XY.

The total forces acting on the wedge OXY are (a) the total force *R* acting across the rupture surface, (b) its weight $W = \frac{1}{2}\gamma a x$, and (c) the lateral force *L* supplied by the wall (which must be horizontal in this case). Suppose that this force *L* is applied through a hydraulic jack, and it is gradually reduced. We see directly from the triangle of forces in Fig. 9.1(a) that the force *R* must gradually be reduced, and more significantly that its inclination to the normal across the plane XY is increased.

At some stage during this process the distributed pressures across the plane XY could have resultants on three segments 1, 2, and 3 as shown in Fig. 9.1(b). We have no knowledge of the actual distribution of stress except for the facts that the polygon of forces in Fig. 9.1(b) must close, and that for each segment the local shear stress τ cannot exceed the limiting magnitude given by eq. (8.1).

However, if the jack force *L* can be reduced until on every segment of this particular rupture surface the limiting condition is reached then the local reactions can be divided into two parts of known magnitude. The force due to cohesion along the segment is proportional to the length of the segment; and in general with *curved* rupture surfaces the resultant of all cohesive reactions equals a cohesive force *C* parallel to the chord of the surface. The frictional reaction is inclined at the limiting angle ρ to the normal to the segment; and in general with curved rupture surfaces, the resultant *F* of all frictional reactions will depend on the distribution of normal pressure. If large normal pressures act at one end of the surface then the overall frictional reaction will be close to the normal to the curve at that end of the surface. However, in the special case of a *plane* surface of rupture the cohesion resultant *C* acts parallel with the plane and the overall frictional resultant *F* acts at an angle ρ to that plane.

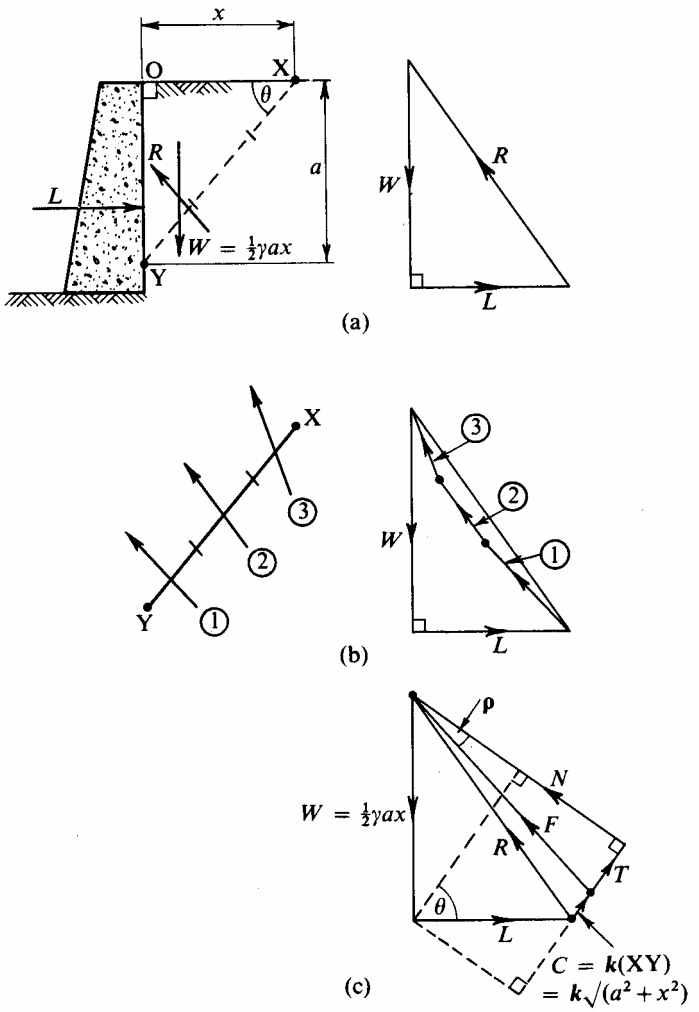

Fig. 9.1 Limiting Equilibrium of a Retaining Wall

So in the limiting case, the total sum of resolved components across each segment of the rupture surface must be as shown in Fig. 9.1(c), such that the total normal force

$$N = L\sin\theta + \tfrac{1}{2}\gamma ax\cos\theta$$

induces a total frictional resistance to sliding of

$$T = F\sin\rho = (L\sin\theta + \tfrac{1}{2}\gamma ax\cos\theta)\tan\rho$$

which together with the total cohesive force $C = k\sqrt{(a^2 + x^2)}$ must be in equilibrium with the resolved components of W and L

$$\tfrac{1}{2}\gamma ax\sin\theta - L\cos\theta.$$

Multiplying through by $\sqrt{(a^2 + x^2)}$ and eliminating θ we get

$$\left(\tfrac{1}{2}\gamma ax^2 + La\right)\tan\rho + k\left(a^2 + x^2\right) = \left(\tfrac{1}{2}\gamma a^2 x - Lx\right)$$

and collecting terms we obtain

$$L = \frac{\tfrac{1}{2}\gamma a^2 x - \tfrac{1}{2}\gamma ax^2\tan\rho - kx^2 - ka^2}{x + a\tan\rho} \tag{9.1}$$

for the *least* lateral force L that can successfully hold up the wedge OXY. If the total lateral force is allowed to fall below L then that particular wedge will actively slide down and increase the lateral force to the value L again.

If we plot L versus x we find the lower curve of Fig. 9.2(a) with a maximum value when

$$0 = \frac{dL}{dx} = \frac{\left(\frac{1}{2}\gamma a \tan\rho + k\right)\left(a^2 - 2ax\tan\rho - x^2\right)}{\left(x + a\tan\rho\right)^2} \tag{9.2}$$

which is satisfied by

$$x = a\tan\varepsilon, \qquad \text{where } \varepsilon = \left(\frac{\pi}{4} - \frac{\rho}{2}\right). \tag{9.3}$$

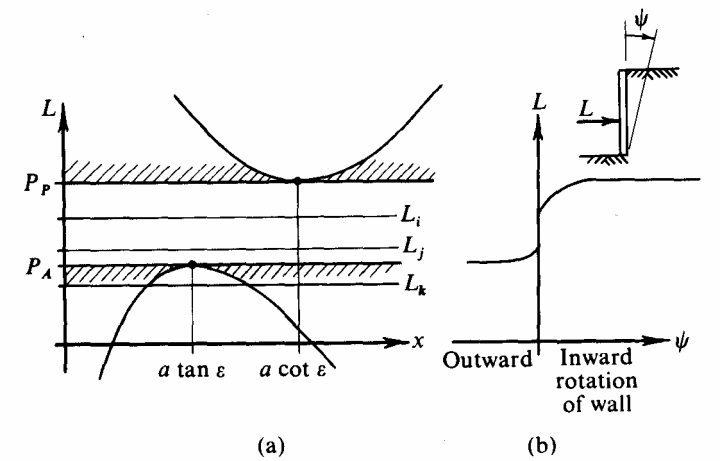

Fig. 9.2 Bounds of Possible Values for Lateral Force on Retaining Wall

The significance of this maximum is as follows. Suppose the lateral force on the jack is slowly reduced and let us represent this by a shift of the faint horizontal lines in Fig. 9.2(a) from value L_i to L_j. The first rupture plane that can become active is the one at $x = a\tan\varepsilon$, inclined to the wall at an angle $(\pi/4 - \rho/2)$. The lateral force cannot fall below this value. If the lateral force could be reduced to L_k there would be two possible rupture planes, but any attempt to reduce the total force will simply be matched by activity of the weakest slip wedge at $x = a\tan\varepsilon$. The magnitude of this active lateral force is found by substituting $x = a\tan\varepsilon$ in the expression for L to give

$$P_A = L = \tfrac{1}{2}\gamma a^2 \tan^2\varepsilon - 2ka\tan\varepsilon \tag{9.4}$$

Where P_A is Coulomb's active lateral pressure force. Coulomb himself published this expression in the form

$$P_A = ma^2 - lka \tag{9.5}$$

and it was the derivation of this equation that was probably Coulomb's major achievement in soil mechanics. He appreciated that for soil without cohesion (k = 0), P_A reduces to $\frac{1}{2}\gamma a^2 \tan^2\varepsilon$, and for soil without cohesion or friction $(k = \rho = 0)$ the active lateral force P_A is $\frac{1}{2}\gamma a^2$ and simply reduces to the fluid force. The presence of friction and cohesion together reduce the active lateral force needed to retain this soil, below that needed to retain a fluid of the same density.

9.2 Coulomb's Analysis of Passive Pressure

Coulomb's calculation was then developed by considering that the lateral force becomes so large that wedges of soil tend to slip upwards along plane surfaces of rupture.

In that case the variation of lateral force L corresponds to the upper curve in Fig. 9.2(a) given by an equation

$$L = \frac{\frac{1}{2}\gamma a^2 x - \frac{1}{2}\gamma a x^2 \tan\rho + kx^2 + ka^2}{x - a\tan\rho} \tag{9.6}$$

which can be obtained directly from the active case by changing the signs of k and ρ throughout. This curve has a minimum at $x = a\cot\varepsilon$ when

$$P_P = \tfrac{1}{2}\gamma a^2 \cot^2\varepsilon + 2ka\cot\varepsilon. \tag{9.7}$$

The significance of this minimum is that when the lateral force rises causing passive resistance of the soil, the first plane of rupture on which slip can occur is the plane inclined to the vertical wall at an angle $(\pi/4 + \rho/2)$. If slip occurs on this plane the soil can continue to resist passively but with lateral force of not more than P_P. This force is in excess of the fluid pressure $\frac{1}{2}\gamma a^2$ because of both friction and cohesion.

In the range of possible lateral force $P_A \le L \le P_P$ the soil is at rest. In the case of cohesionless soil with $\rho = 30^\circ, \tan^2\varepsilon = \frac{1}{3}$ and the ratio $P_P/P_A = 9$. This very wide range of possible values of L makes it necessary to introduce some additional consideration if a close estimate of a value of L is to be made. For example, in Coulomb's design free-standing walls withstand a lateral force 1.25 P_A without overturning. It is recognized that the lateral force L may well exceed this design value but if it does so, it is supposed that a little outward movement of the wall will relieve the lateral force, which will then fall to the design value. In several experiments on large model retaining walls Terzaghi[2] did establish this effect of Fig. 9.2(b); after a very small outward rotation (0.001 radian) of a retaining wall the lateral force fell to the active value, but much larger inward rotation (0.1 radian) was required before the lateral force approached the passive pressure. A phrase common in the literature is that the strains required to 'mobilize the strength' of the ground are large in the passive case and small in the active case.

However, we must not forget that Coulomb's calculation does not in itself contain any mention of the *magnitude* of strains or displacements. All that is specified is the *direction* of incipient movement on the slip plane as shown in Fig. 9.3.

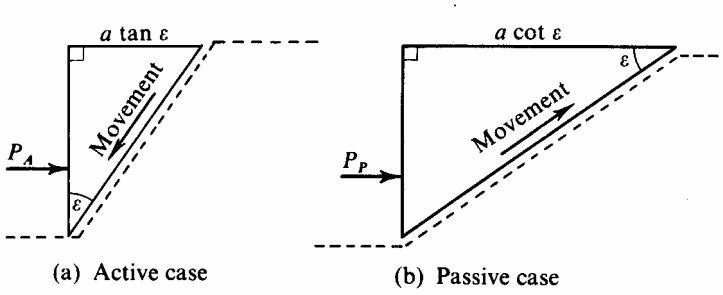

Fig. 9.3 Slip Planes for Active and Passive Failures

By putting $P_A = 0$ in the eq. (9.5) for the active force

$$0 = P_A = \frac{1}{2}\gamma a^2 \tan^2\varepsilon - 2ka\tan\varepsilon$$

Coulomb found the height to which a face could stand unsupported to be

$$a \le \frac{4k}{\gamma\tan\varepsilon}; \tag{9.8}$$

and a face of this height would certainly fail under its own self- weight. He went on to consider whether a larger active force (or a lower unsupported height of a vertical face)

would be found for some surface of sliding other than plane (Fig. 9.4) and introduced the important idea of using vertical slices to find the pressures on a curved rupture surface. Unfortunately, he was writing before the nature of stress in a continuum was well understood and he wrongly supposed that he needed to specify limiting stresses both on the rupture surface and on the vertical planes between slices; this error prevented Coulomb from making a successful development of the method of slices.

It is clearly possible to extend this simple method of analysis to obtain general solutions to problems where the retaining wall is battered, or rough, or the backfill is not horizontal or consists of several different strata.

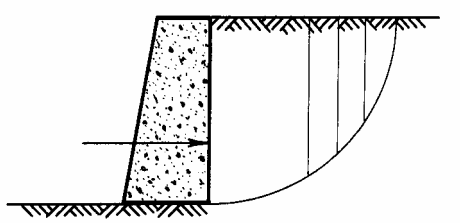

Fig. 9.4 Possible Curved Failure Surface Considered by Coulomb

9.3 Coulomb's Friction Circle and its Development in Gothenberg

In 1785 Coulomb wrote a prize paper[3] on problems of cordage and rigging of ships. This paper included the solution to the problem of slip of ropes round frictional bollards, and the solution to the problem of the torsion of round spars. The paper also introduced the friction circle construction for analysis of the slip of a shaft, Fig. 9.5, in a frictional plane bearing. The shaft turns and slips along a line contact such that the reaction is inclined to the radius R at the friction angle ρ. Conveniently a 'friction circle' of radius $R \sin \rho$ is drawn, and a graphical construction is made in which the limiting reaction is tangential to the friction circle. Coulomb's technique of 1785 was to be applied in 1916 to the problem of slip of soil on circular surfaces of rupture[4] by the engineers of the Swedish port of Gothenberg where there was a series of failures of the quay walls.

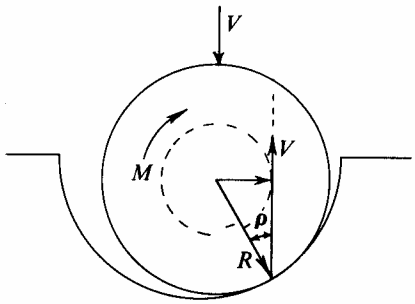

Fig. 9.5 Circular Shaft about to Slip

One successful design of quay wall, Fig. 9.6(a), was based on the consideration of straight planes of sliding. In Fig. 9.6(b) the active force A, due to pressure of retained soil and superposed traffic, is made small by placing highly frictional gravel behind the wall; and the passive force P, due to resistance of a wedge of soil in front of the toe of the quay, is made large by placing highly frictional gravel there also. The next quay wall, shown in Fig. 9.7, should have been by these considerations more stable than its forerunner; the clay below this new fill was considered to be stiffer than at the former site, and yet 'the quay wall slid slowly into the river in March 1916 just before it was completed and before any live load had been added to the quay area'. Borings and other observations showed that the

movement approximated to slip on a circular surface of sliding through the clay below the gravel fill. Yet another large quay wall was under construction for the Central Harbour and this failure made it imperative for the engineers concerned to revise their design principles.

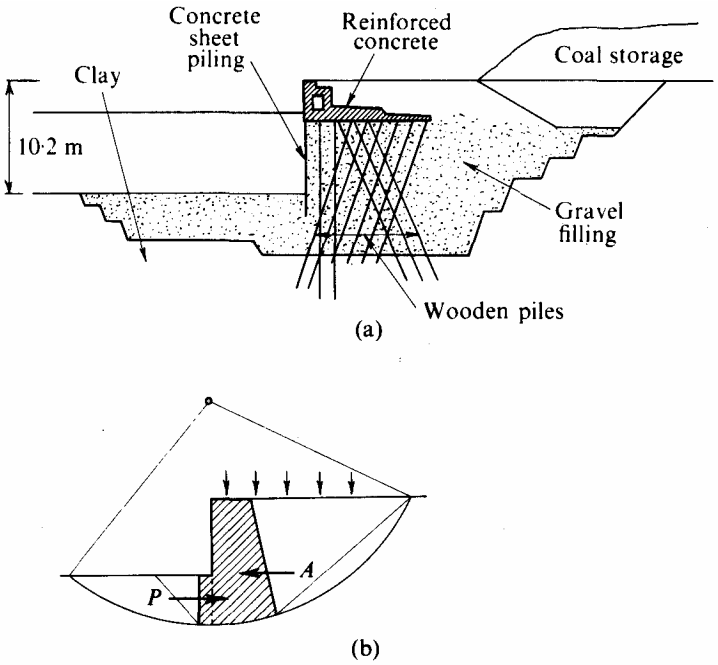

Fig. 9.6 Quay at the Sannegard Harbour 1914 (After Petterson)

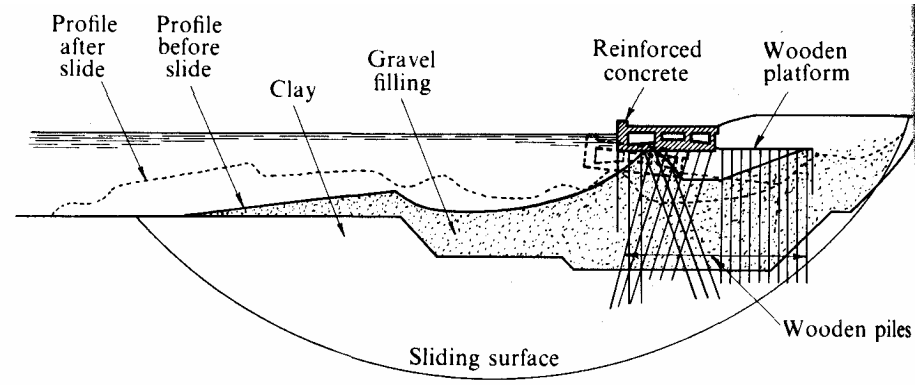

Fig. 9.7 The Stigberg Quay, Sliding Surface, 1 916 (After Petterson)

Their investigation was based on the general view held at that time, that friction governed the behaviour of all kinds of soil and that a graphical method of polygons of force was the most practical basis for the analysis. An existing gravel fill in the Central Harbour project was extended to form a test load: when this test was in the stage shown in Fig. 9.8 a crack was observed in the fill and the soil moved slowly about 17 cm outward and 25 cm downwards and did not come to rest for 9 days. Analysis of the failures of both the quay wall and test load was made in the manner shown in Fig. 9.8.

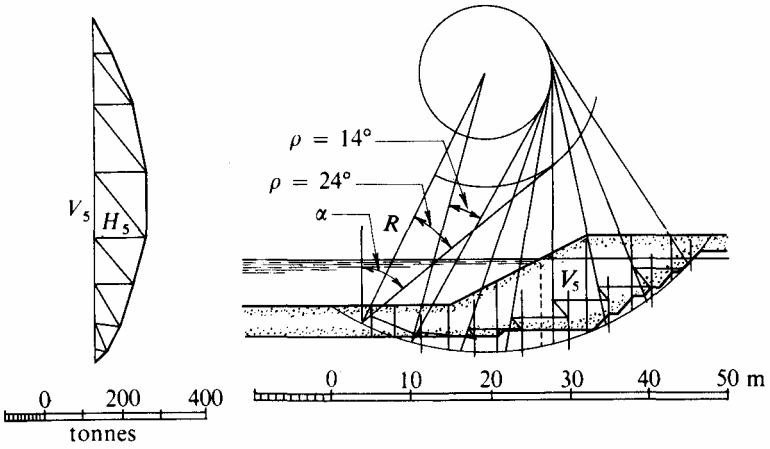

Fig. 9.8 Investigation of Stability under the Test Load in the Free Harbour, 1916 (After Petterson)

A possible circular sliding surface of radius R was drawn through the ground, the cross-section within the circle divided into vertical slices, and the vertical weight V and centre of gravity determined for each slice. A horizontal force H was assumed to act between slices at the lower third point of the interface. A tentative value was assumed for the friction angle effective along the circular arc and a friction circle of radius R sin ρ was drawn. For each slice number n the vertical weight V, was known, and the frictional reaction across the base of the slice had to be in a direction tangential to the friction circle inclined at an angle α_n to the vertical. Hence the difference between the horizontal forces to either side of this slice was

$$H_n - H_{n-1} = V_n \tan \alpha_n.$$

The force polygon of Fig. 9.8 was constructed starting from the first slice; when the last slice was reached the polygon should close with no horizontal reaction to the right. Trials with different values showed what frictional angle ρ was required just to maintain equilibrium of the sliding mass within that particular circular surface of sliding. Then many other possible sliding surfaces were thus analysed and it was considered that the surface which required the *largest* value of ρ was the most critical and failure would occur first along it. In the analysis of the Central Harbour failure of Fig. 9.8, a frictional angle ρ = 24° was assumed for the part of the sliding surface that passed through the gravel, and the largest value of ρ required for stability of the clay was found to be about 14°. For the quay wall failure of Fig. 9.7 the value of ρ required for stability was about 10°.

The analysis of these failures made it clear that quay walls with heavy gravel fills were unsuitable for that particular clay foundation. The design for the new quay wall in the Central Harbour was modified as shown in Fig. 9.9(a). The weight of gravel filling in front of the quay wall was unaltered but the weight below the quay was reduced; the quay became a loading platform resting on wooden piles that were driven down through a gravel slope into the underlying clay. The factor of safety of the new design was estimated as follows. The force polygon was started from both ends. A division was introduced at the vertical plane tangential to the friction circle. All slices to the right of this plane were considered to be actively causing an increase of horizontal force between slices, and the worst case included traffic loading on these slices; all slices to the left of this plane were considered to be passively resisting the horizontal force from the right and the worst case allowed no traffic loading on these slices. The polygons completed from each end up to this vertical plane gave a horizontal force H_A active from the right and a horizontal force

H_P available in passive resistance to the left. The ratio H_P/H_A was regarded as the factor of safety of the design: in the Central Harbour design this factor was about $1\frac{1}{2}$, and in another case a factor of $1\frac{1}{3}$ was considered satisfactory.

The method of slices was clearly capable of extension. Non circular surfaces could later be considered, and the division between 'active and passive slices' would then simply be found by drawing a tangent at slope ρ to the curve of sliding. Cohesion could also be considered and a suitable polygon of forces quite simply found. The effect of pore-pressure in producing variation of effective normal stress across the sliding surface was later introduced. Other later definitions of factor of safety included a ratio of moments taken about the centre of the circle of 'disturbing' active forces and 'restoring' passive forces.

An extensive literature[5–8] has been written on the analysis of equilibrium on rupture surfaces. When referring to these texts the reader should be careful to note what assumption each writer makes about distributions of pore-pressure and of total normal pressure along any assumed rupture surface, and what definition is used for factors of safety. In each of these respects a certain variation of practice exists.

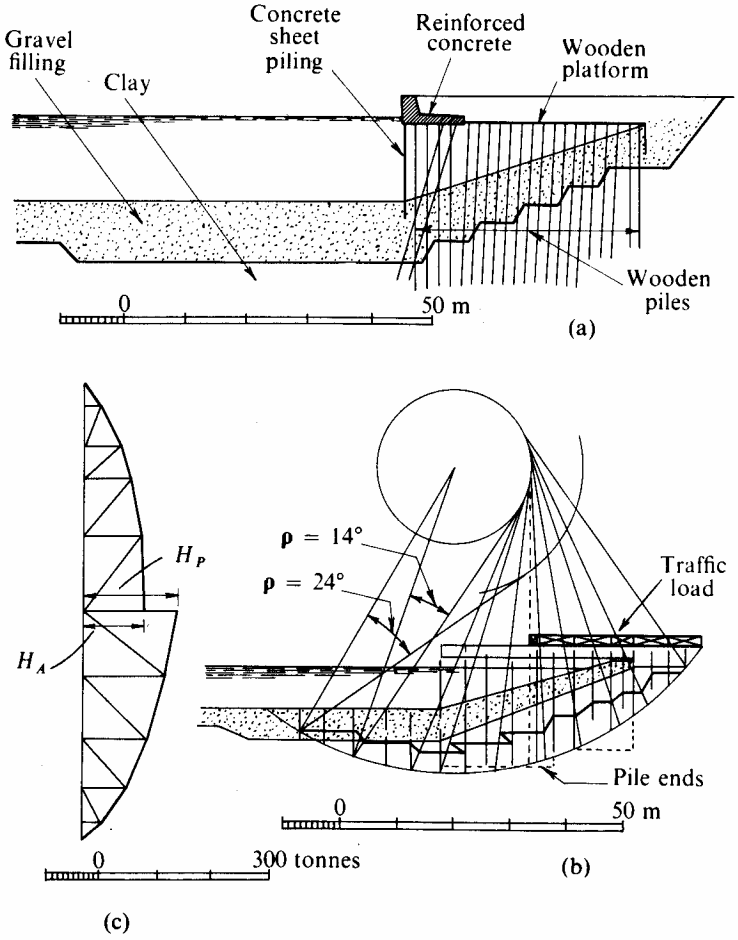

Fig. 9.9 Quay in the Free Harbour as built, and Evaluation of the Stability of the Quay in the Free Harbour, 191 6 (After Petterson)

9.4 Stability due to Cohesion Alone

Only a few years after the original analysis of the slips at Gothenberg alternative analyses were developed based on cohesion alone.

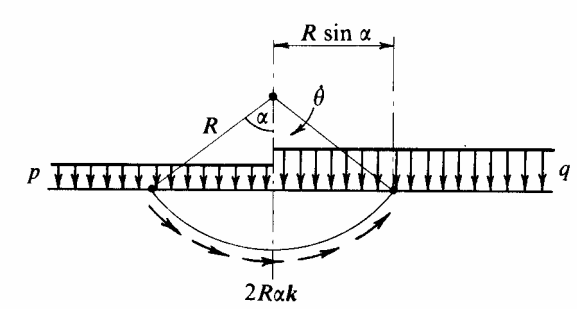

Fig. 9.10 Cylindrical Slip Surface in Clay

In Fig. 9.10 we show the section of a semi-infinite half-plane of homogeneous clay loaded to the right with a uniformly distributed load q and to the left with a uniformly distributed load p. Here we are again introducing nomenclature which will enable the reader to gain more ready access to Sokolovski's *Statics of Granular Media.*[9] No confusion need arise with the use of p and q in earlier chapters. The problem is analysed on the supposition that the clay ruptures and rotates clockwise on a cylindrical slip surface which will be assumed of unit length perpendicular to the section. All normal reactions on the slip surface pass through the centre of the slip-circle, and all tangential reactions are simply of magnitude k per unit length of arc. It is clear that the worst circles have centres over the edge which divides the loading, since any extension of q to the left or p to the right will reduce the loading power available for dissipation.

Let the family of circles with centres over the edge be determined by the parameter α, the half-angle shown in Fig. 9.10. During a small clockwise rotation of $\dot{\theta}$ it is assumed that the total power of the descending load less the power of the rising load must equal the power dissipated in overcoming cohesion on the cylindrical slip surface. The distance moved by the centre of gravity of both moving loads is $(\frac{1}{2}R\sin\alpha)\dot{\theta}$ so that

$$(q-p)R\sin\alpha(\tfrac{1}{2}R\sin\alpha)\dot{\theta} = k2R\alpha R\dot{\theta},$$

i.e.,
$$(q-p) = k\frac{4\alpha}{\sin^2\alpha}. \tag{9.9}$$

This expression for $(q-p)$ has a minimum when

$$0 = \frac{\mathrm{d}}{\mathrm{d}\alpha}\left(\frac{\alpha}{\sin^2\alpha}\right) = \operatorname{cosec}^2\alpha - 2\alpha\operatorname{cosec}^2\alpha\cot\alpha,$$

i.e., when
$$\tan\alpha = 2\alpha \tag{9.10}$$

which is satisfied by $\alpha = 1.1656 \text{ rad} = 66^\circ 47'$. On substitution in eq. (9.9) this gives, for the worst case, a maximum loading differential

$$(q-p)_{\max} = 5.53k. \tag{9.11}$$

Let us apply this result to the stability of river banks. In general a river bank may be most inclined to fail locally, as in Fig. 9.11, with a weight W of soil slipping round the circular arc AB. The resultant of the cohesion k round the arc AB is then equal to a force K parallel to the chord AB; the weight W simply depends on the geometry of the section and the unit weight γ of the soil. The triangle of forces shown in Fig. 9.11 indicates a value of $\boldsymbol{k}$ needed just to satisfy statical equilibrium. However, when slope protection works are put in hand and a well drained bank or an anchored sheet-pile wall or piled quay is built over purely cohesive ground, the possibility of deep-seated failure places an overall restriction on the difference of level or of loading that can be carried.

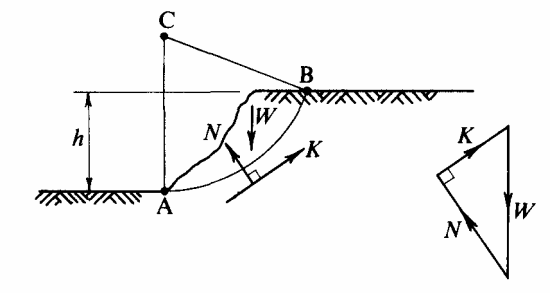

Fig. 9.11 Local Failure of River Bank

For example, imagine in Fig. 9.12 a wide river passing across land where there is a considerable depth of clay with cohesion k = 3 tonnes/m^2 and of saturated weight 16 tonnes/m^3. If the difference of level between the river banks and the river bed was h, then (ignoring the strength of the clay for the portion BD of the sliding surface,

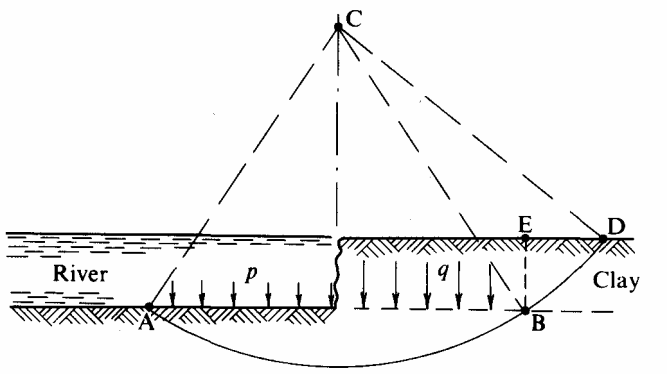

Fig. 9.12 Deep-seated Failure of River Bank

and the weight of the wedge BDE) for an approximate calculation we have $q = 1.6h$ and $p = \gamma_w h = 1.0h$ when the river bed was flooded or $p = 0$ when the river bed was dry giving in the worst case $(q - p) = 1.6h$. We also have from eq. (9.11)

$$(q - p)_{\max} = 5.53k = 16.6 \text{ tonnes/m}^2 \tag{9.12}$$

so that $$h \le \frac{16.6}{1.6} = 10\,\text{m, say}$$

which gives one estimate of the greatest expected height of the river banks. If the river were permanently flooded the depth of the river channel could on this basis be as great as

$$\frac{16.6}{0.6} \cong 27.6\,\text{m.} \tag{9.13}$$

An extensive literature has been written on the analysis of slip-circles where the soil is assumed to generate only cohesive resistance to displacement. We shall not attempt to reproduce the work here, but instead turn to the theory of plasticity which has provided an alternative approach to the solution of the bearing capacity of purely cohesive soils.

9.5 Discontinuity Conditions in a Limiting-stress Field

In this and the next section we have two purposes: the principal one is to develop an analysis for the bearing capacity problem, but we also wish to introduce Sokolovski's notation and provide access to the extensive range of solutions that are to be found in his *Statics of Granular Media.* In this section we concentrate on notation and develop simple conditions that govern discontinuities between bodies of soil, each at some Mohr—

Rankine limiting stress state: in the next section we will consider distribution of stress in a region near the edge of a load — a so-called 'field' of stresses that are everywhere limiting stresses.

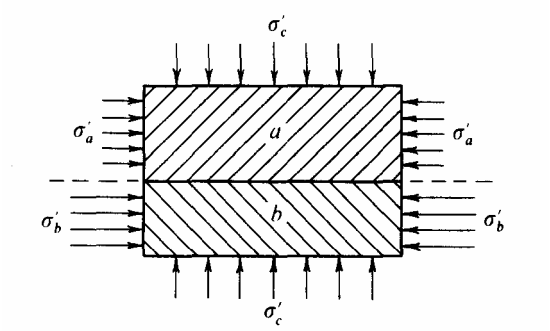

Fig. 9.13 Two Rectangular Blocks in Equilibrium with Discontinuity of Stress

In Fig. 9.13 we have a section through two separate rectangular blocks made of different perfectly *elastic* materials, *a* and *b,* where material *b* is stiffer than *a.* The blocks are subject to the boundary stresses shown, and if σ'_a and σ'_b are in direct proportion to the stiffnesses E_a and E_b then the blocks are in equilibrium with compatibility of strain everywhere. However, the interface between the blocks acts as a *plane of discontinuity* between two states of stress, such that the stress σ'_c across this plane must be continuous, but the stress parallel with the plane need not be.

In a similar way we can have a plane of discontinuity, *cc,* through a single perfectly *plastic* body such as that illustrated in Fig. 9.14(a). Just *above* the plane *cc* we have a typical small element *a* experiencing the stresses (σ'_a, τ_{ac}) and (σ'_c, τ_{ca}) which are represented in the Mohr's diagram of Fig. 9.14(b) by the points A and C respectively on the relevant circle *a*.

Just *below* the plane *cc* the small element *b* is experiencing the stresses (σ'_b, τ_{bc}) and (σ'_c, τ_{cb}) which are represented by the points B and C respectively on the relevant Mohr's circle *b.* In order to satisfy equilibrium we must have $\tau_{ac} \equiv \tau_{ca} \equiv \tau_{bc} \equiv \tau_{cb}$ but as before there is no need for σ'_a to be equal to σ'_b. Since the material is perfectly plastic there is no requirement for continuity or compatibility of strain across the plane *cc.*

We can readily obtain from the respective Mohr's circles the stresses acting on any plane through the separate elements a and *b;* and in Fig. 9.14(c) the principal stresses are illustrated. The key factor is that there is a marked jump in both the *direction* and *magnitude* of the major (and minor) principal stresses across the discontinuity — and this will be the essence of the plastic stress distributions developed in the remainder of this chapter. This will be emphasized in all the diagrams by showing the major principal stress in the form of a vector, and referring to it always as Σ'.

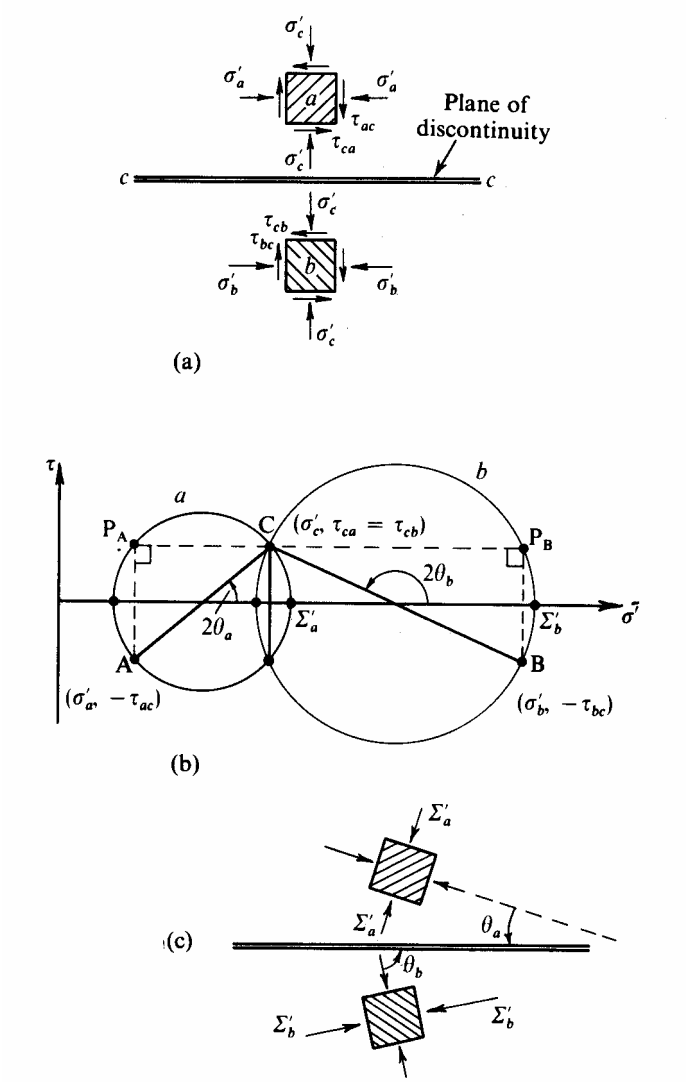

Fig. 9.14 Perfectly Plastic Body Containing Stress Discontinuity

In Fig. 9.15(a) we see a section through a plane body of soil across which there act stress components n normal and τ tangential to the section. These components define a point P in the stress plane of Fig. 9.15(b), in which we see also the Mohr—Rankine limiting lines

$$|\tau| = k + \sigma' \tan\rho,$$

intersecting the axis at O where OJ = k cot ρ = H. It proves convenient to transform all problems to equivalent problems of either perfectly frictional or perfectly cohesive soil. So in cases where $\rho \neq 0$ Sokolovski introduces an additional pressure H as well as the stress components n and t, and in Fig. 9.15(c) the *equivalent* stress (remembering that the symbols p and q are used by Sokolovski and in this chapter only for distributed loading on some planes) p' is such that $p'\sin\delta = t$ and $p'\cos\delta = (n + H)$.

In Fig. 9.16(a) there are seen to be two alternative circles of *limiting* stress through the point P. One circle has centre Q_+ and the other has centre Q_-. The line OP cuts these circles as shown in Fig. 9.16(a) and the angle Δ is such that

$$\sin\Delta = \frac{\sin\delta}{\sin\rho} \quad (\rho \neq 0). \tag{9.14}$$

We must be careful about the sign conventions associated with the definition of Δ. The angle of friction ρ is a material constant and is always positive (or zero), so that the sign of Δ is always the same as δ. All angles in Mohr's diagram are measured positive in an anticlockwise direction so that positive δ and Δ are associated with positive shear stress τ; in particular when P is below the σ'-axis, $\Delta<0$.

Use of this angle Δ was suggested by Caquot and was then brought in to the second edition of *Statics of Granular Media.*

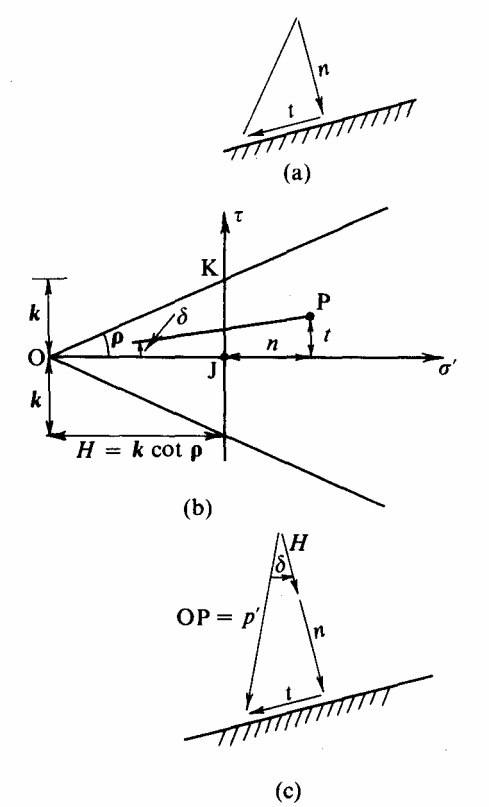

Fig. 9.15 Sokolovski's Equivalent Stress

Another symbol that figures extensively in the book is $\kappa = \pm 1,$ in such contexts as

$$\left.\begin{aligned} \sigma' &= p'\frac{\sin\Delta}{\sin(\Delta-\kappa\delta)} \\ \text{where}\quad \kappa=+1 \text{ gives } \sigma'_{+} &= \mathrm{OQ}_{+} = \mathrm{OP}\frac{\sin\Delta}{\sin(\Delta-\delta)} \\ \text{and}\quad \kappa=-1 \text{ gives } \sigma'_{-} &= \mathrm{OQ}_{-} = \mathrm{OP}\frac{\sin\Delta}{\sin(\Delta+\delta)}. \end{aligned}\right\} \qquad (9.15)$$

This convenient notation permits Sokolovski to write general equations, and to distinguish between a *maximal* limiting-stress state when $\kappa=+1$ and a *minimal* limiting-stress state when $\kappa=-1$. These alternative states can exist cheek by jowl, facing each other across a discontinuity on which the stress components n and t act as in Fig. 9.16; this case represents the biggest allowable jump or change in stress across the discontinuity.

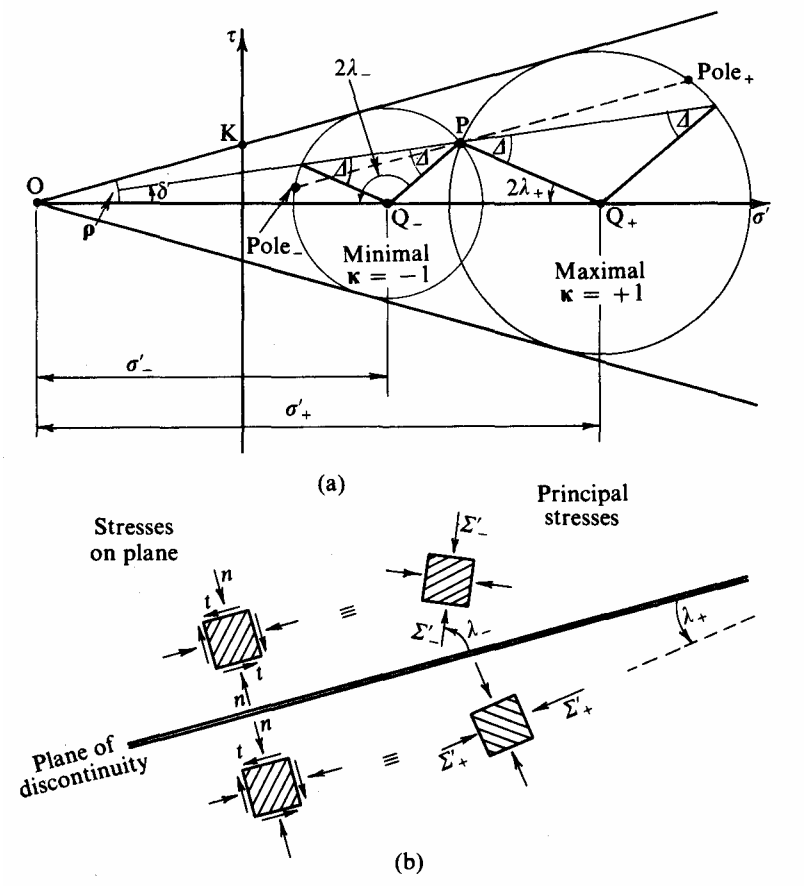

Fig. 9.16 Maximal and Minimal Limiting Stresses

The first condition that applies to these limiting stress states is that the shift in centre of the stress circles must satisfy the condition

$$\frac{\sigma'_+}{\sigma'_-} = \frac{\sin(\Delta + \delta)}{\sin(\Delta - \delta)} \qquad (9.16)\ \text{cf. Sokolovski (2.42)}$$

A second condition is that the change in inclination of the direction of the major principal stress Σ' also depends on Δ. In Fig. 9.16(b) we define the *anticlockwise* angles* *from* the direction of the discontinuity to the directions of Σ' on either side as λ_- and λ_+. The general condition is

$$2\lambda = (1-\kappa)\frac{\pi}{2} + \kappa\Delta - \delta + m\pi \qquad (9.17)\ \text{cf. Sokolovski (1.17)}$$

where m is an integer, chosen to agree with the sign convention for λ.

For $\kappa = +1$ we have $2\lambda_+ = \Delta - \delta$

$\kappa = -1$ we have $2\lambda_- = \pm\pi - \Delta - \delta$

where the + sign is associated with positive shear ($\delta > 0$) and the – sign is associated with negative shear ($\delta < 0$). The second condition applying to the discontinuity is therefore

$$\lambda_- - \lambda_+ = \pm\frac{\pi}{2} - \Delta \qquad (9.18)$$

* This is a minor departure from Sokolovski who measures the *clockwise* angle from Σ' *to* the discontinuity: it makes no difference to the mathematical expressions but means all angles have a consistent sign-convention.

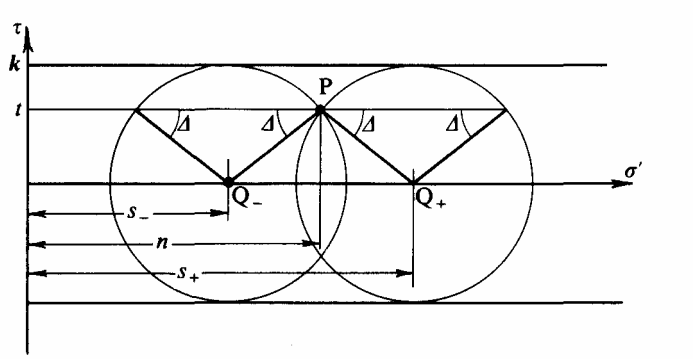

Fig. 9.17 Limiting-stress Circles for Purely Cohesive Material

If we consider instead the case of a perfectly cohesive soil (ρ=0) we have the situation of Fig. 9.17 for which this second condition remains valid. However, the first condition of eq. (9.16) must be expressed as

$$\frac{\sigma'_+}{\sigma'_-} = \frac{s_+ + H}{s_- + H} = \frac{\sin(\Delta + \delta)}{\sin(\Delta - \delta)}$$

so that as $\delta \to 0 (\text{and} \sigma'_+, \sigma'_-, p' \text{and} H \text{ each} \to \infty)$ it can be expanded to give

$$s_+ - s_- = 2k\cos\Delta. \qquad (9.19) \text{ cf. Sokolovski (4.32)}$$

We also have to redefine Δ in the form

$$\sin\Delta = \frac{t}{k} \quad (\rho = 0). \qquad (9.20)$$

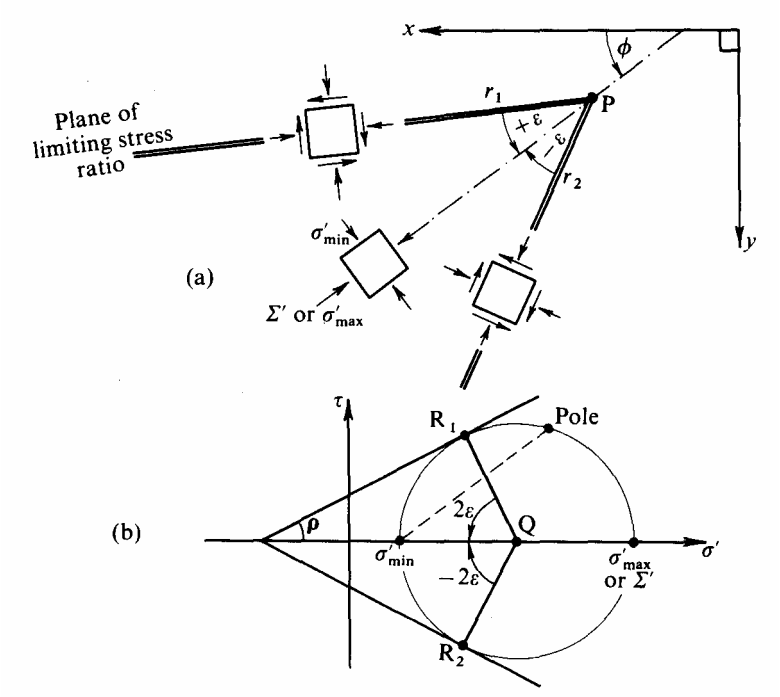

Fig. 9.18 Planes of Limiting-stress Ratio

We will be dealing with a number of discontinuities all at different inclinations, so it becomes important to have a pair of fixed reference axes. Sokolovski uses Cartesian coordinates x horizontal and positive to the left, and y vertical and positive downwards which is consistent with our sign convention for Mohr's circle (appendix A). The angle ϕ is defined to be the anticlockwise angle between the x-axis and the direction of major

principal stress Σ' in Fig. (9.18). This angle will play a large part in the remainder of this chapter, and should not be confused with its widespread use in the conventional definition for the angle of friction.

In Fig. 9.18(a) we have a point P in a perfectly plastic body in a state of limiting stress, with appropriate Mohr's circle in Fig. 9.18(b). From this we can establish the direction of the major principal stress Σ' and the directions r_1 and r_2 of the planes of limiting stress ratio. The angle between these is such that $\varepsilon = (\pi/4 - \rho/2)$ and this agrees with the definition in eq. (9.3) in §9.2 on Coulomb's analysis.

In order to define a limiting-stress state in soil of given properties **(*k*, ρ)** only two pieces of information are needed: one is the position of the centre of the stress circle, either σ' or *s,* and the other is the direction of major principal stress relative to the horizontal *x*-axis described by ϕ. Across a discontinuity the change of the values of these data is simply related to Δ, which is defined by eqs. (9.14) and (9.20).

9.6 Discontinuous Limiting-stress Field Solutions to the Bearing Capacity Problem

We can now turn to the bearing capacity problem. Previously, in §9.4 when we considered the possibility of circular rupture surfaces, we only attempted to specify the distribution of stress components across the sliding surface. In this section we will be examining the same problem on the supposition that there are discontinuities in the distribution of stress in the soil near a difference of surface loading, and we will fully specify limiting-stress states in the whole of the region of interest.

We shall simplify the problem by assuming the soil is weightless $(\gamma = 0)$, but we will see later that this is an unnecessary restriction and that the analysis can be extended to take account of self-weight. The cases of (a) purely frictional and (b) purely cohesive soils need to be considered separately, and the latter, which is easier, will be taken first.

9.6.1. *Purely cohesive soil* $(\rho = 0, \gamma = 0)$

Figures 9.19(a), 9.20(a), and 9.21(a) show a section of a semiinfinite layer of uniform soil supporting a known vertical stress *p* applied to the surface along the positive *x*-axis. The problem is to estimate the maximum vertical stress *q* that may be applied along the negative *x*-axis. In the limiting case the stress *p* must be a minor principal stress so that the associated major principal stress Σ' must be in a *horizontal* direction $(\phi = 0)$. In contrast, the stress *q* will be itself a major principal stress in the *vertical* direction $(\phi = \pi/2)$, so that somewhere in the vicinity of the *y*-axis we must insert one or more discontinuities across which the value of ϕ can change by π/2.

If we have *n* discontinuities it is simplest to have *n* equal changes of ϕ, i.e., $\delta\phi = +(\pi/2n)$ at each discontinuity. With the boundary conditions of Fig. 9.19 we shall be concerned with *negative* shear, i.e., $\Delta \le 0$, so that we select from eq. (9.18)

$$(\phi_- - \phi_+) = (\lambda_- - \lambda_+) = -\frac{\pi}{2} - \Delta$$

and for *each* discontinuity

$$\Delta = -\frac{\pi}{2} + \phi_+ - \phi_- = -\frac{\pi}{2} + \delta\phi = -\frac{\pi}{2} + \frac{\pi}{2n} = \frac{\pi}{2}\left(\frac{1}{n} - 1\right). \tag{9.21}$$

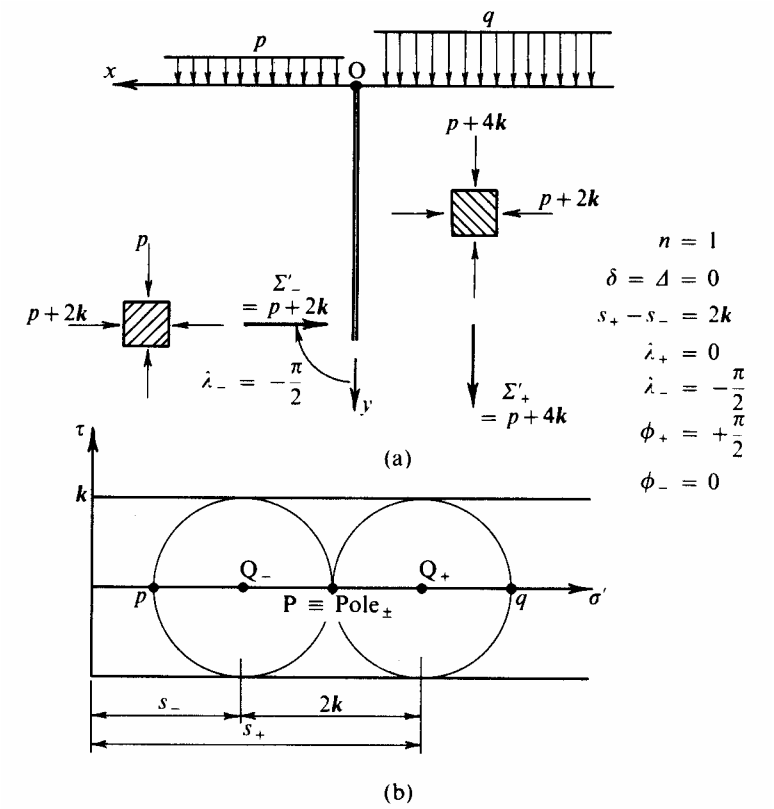

Fig. 9.19 Limiting-stress Field with One Discontinuity for Cohesive Soil

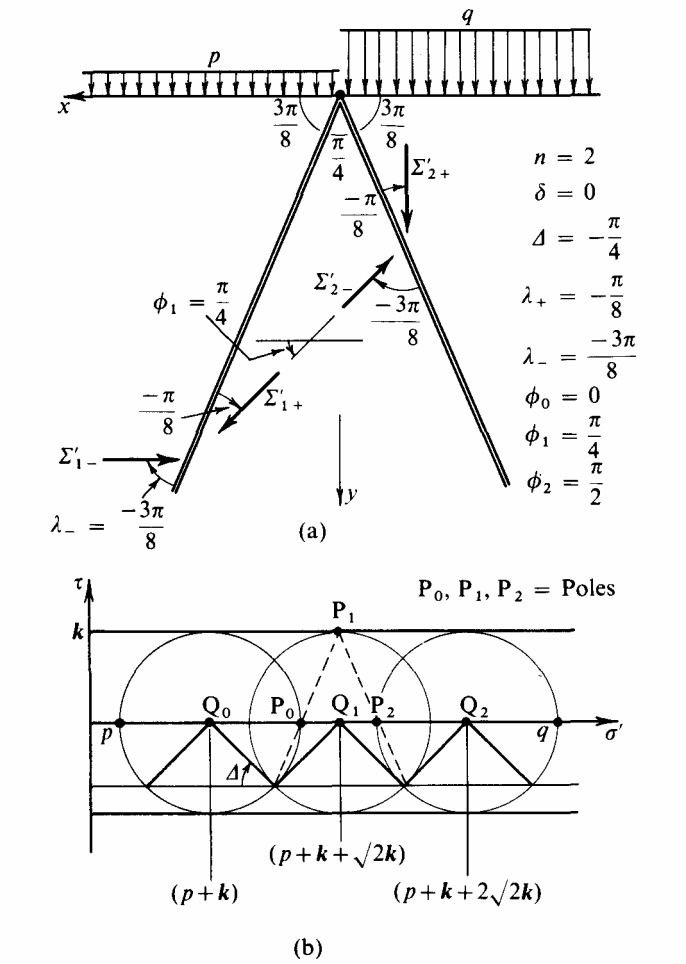

Fig. 9.20 Limiting-stress Field with Soil Discontinuities for Cohesive soil

Substituting in eq. (9.19) we have for the shift of Mohr's circles

$$(s_+ - s_-) = 2k\cos\Delta = 2k\cos\frac{\pi}{2}\left(\frac{1}{n}-1\right) = 2k\sin\frac{\pi}{2n} = 2k\sin\delta\phi. \tag{9.22}$$

The case of a *single* discontinuity $(n=1)$ is fully illustrated in Fig. 9.19, for which $\Delta = 0$ and the two stress circles have centres separated by a distance 2k. The corresponding value of q is $p + 4k$.

For the case of *two* discontinuities ($n = 2$) in Fig. 9.20, $\Delta = -\pi/4$ and the three stress circles have centres spaced $\sqrt{(2)}k$ apart giving $q_{\max} = p + 2k + 2\sqrt{(2)}k = p + 4.83k$.

When n becomes *large,* Fig. 9.21, it is convenient to adopt the differentials from eqs. (9.21) and (9.22)

$$\Delta = -\frac{\pi}{2} + \delta\phi$$

and

$$\delta s = s_+ - s_- = 2k\sin\delta\phi = 2k\ \delta\phi$$

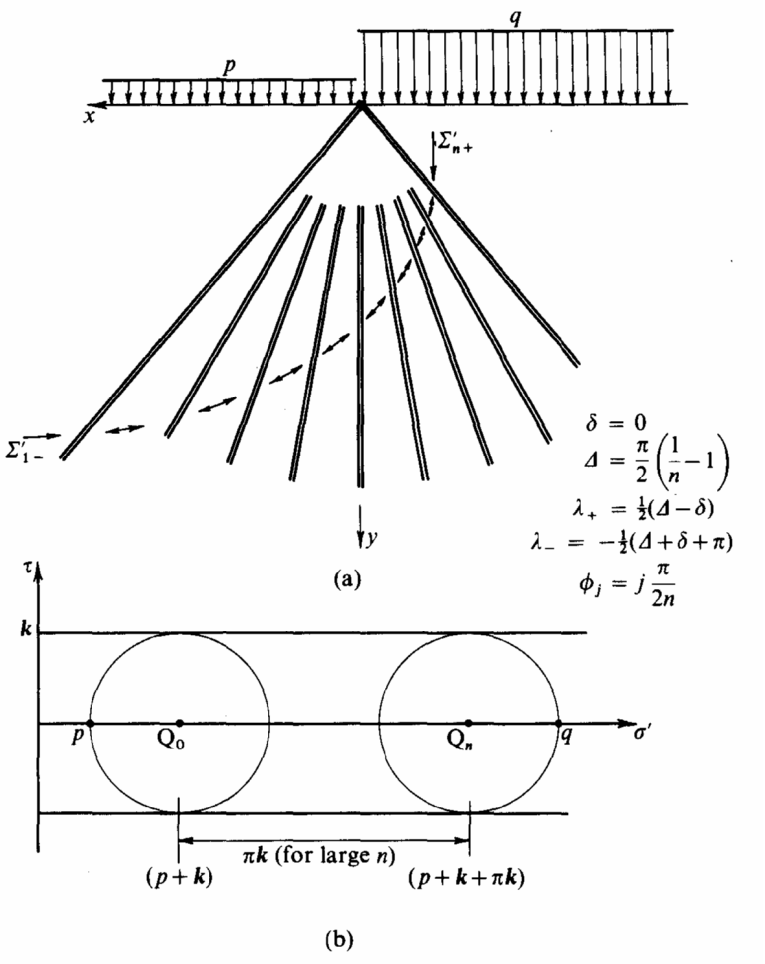

Fig. 9.21 Limiting-stress Field with *n* Discontinuities for Cohesive Soil

which are illustrated in Fig. 9.22(a). Integrating, we find that the total distance apart between the centres of the extreme stress circles becomes

$$\int \mathrm{d}s = \int_0^{\pi/2} 2k\,\mathrm{d}\phi = \pi k$$

leading to $q_{\max} = p + 2k + \pi k = p + 5.14k$.

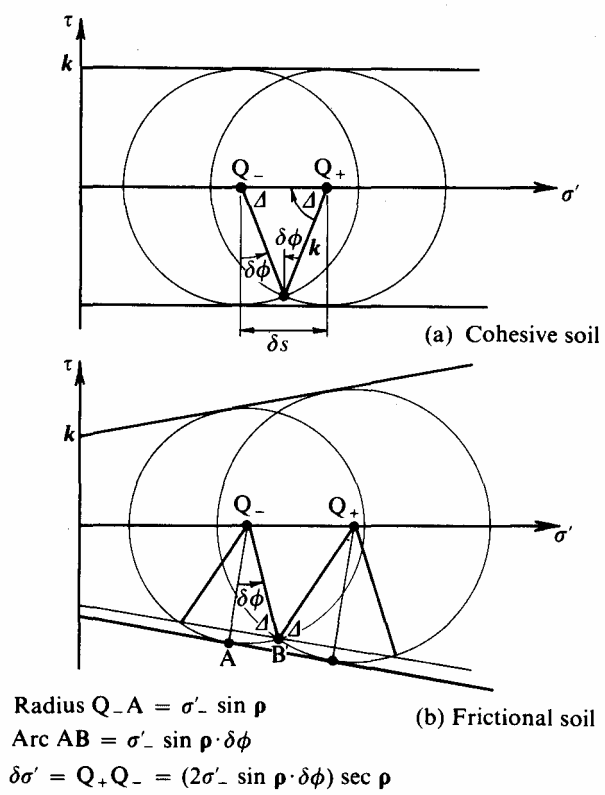

Fig. 9.22 Shift of Limiting Stress Circles for Small Change of ϕ

9.6.2 *Purely frictional soil* $(k = 0, \gamma = 0)$

Figures 9.23(a), 9.24(a), and 9.25(a) illustrate successive solutions to the same problem for n= 1, n=2, and large n except that the soil is now purely frictional. As before, we shall have a change of ϕ of $(\pi/2n)$ at each discontinuity, and negative shear $(\Delta \le 0)$ so that

$$\Delta = -\frac{\pi}{2} + \delta\phi = \frac{\pi}{2}\left(\frac{1}{n} - 1\right).$$

This must be substituted into the appropriate equation, (9.16), to give

$$\frac{\sigma'_+}{\sigma'_-} = \frac{\sin(\Delta + \delta)}{\sin(\Delta - \delta)} = \frac{\sin\Delta\cos\delta + \cos\Delta\sin\delta}{\sin\Delta\cos\delta - \cos\Delta\sin\delta}$$

and introducing $\sin\delta = \sin\Delta\sin\rho$ we obtain

$$\frac{\sigma'_+}{\sigma'_-} = \frac{\cos\delta + \cos\Delta\sin\rho}{\cos\delta - \cos\Delta\sin\rho} = \frac{\cos\delta + \sin\dfrac{\pi}{2n}\sin\rho}{\cos\delta - \sin\dfrac{\pi}{2n}\sin\rho} \tag{9.23}$$

For a *single* discontinuity when $n = 1, \delta = \Delta = 0$ and the two stress circles are spaced so that

$$\frac{\sigma'_+}{\sigma'_-} = \frac{1 + \sin\rho}{1 - \sin\rho};$$

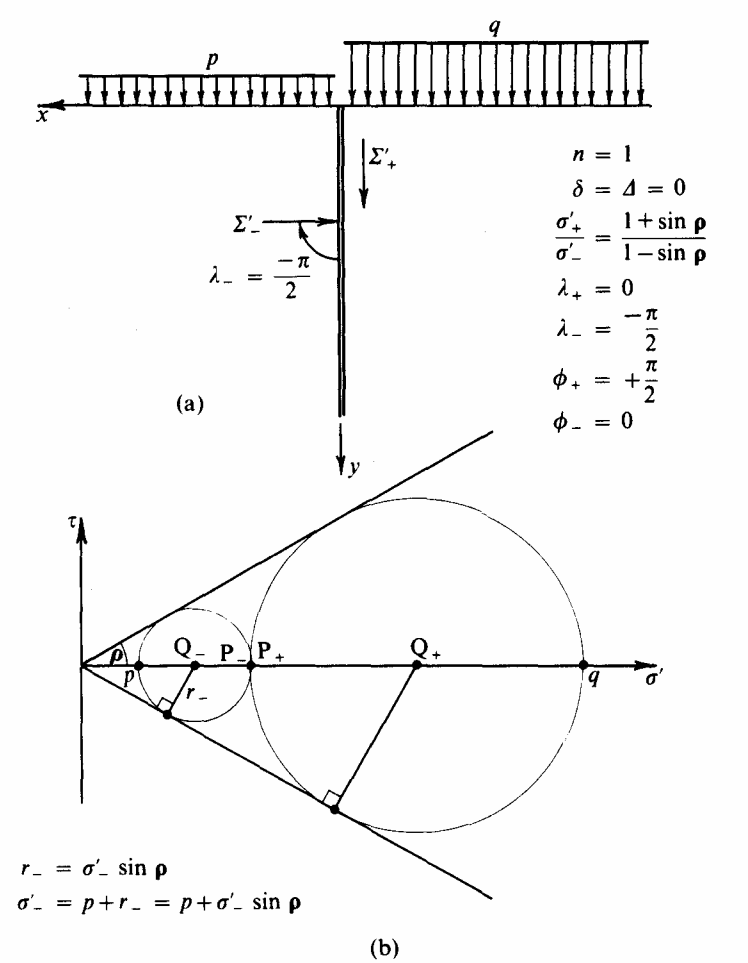

Fig. 9.23 Limiting-stress Field with One Discontinuity for Frictional Soil

in addition

$$p = \sigma'_{-}(1-\sin\rho)$$

$$q = \sigma'_{+}(1+\sin\rho)$$

which leads to

$$q_{\max} = p\left(\frac{1+\sin\rho}{1-\sin\rho}\right)^2.$$

To take a specific example, if ρ = 30° then $q_{\max} = 9p$.

For *two* discontinuities when

$$n = 2, \quad \Delta = -\pi/4, \qquad \sin\delta = -(1/\sqrt{2})\sin\rho$$

and on substitution in eq. (9.23) we can obtain

$$\frac{\sigma'_1}{\sigma'_0} = \frac{1+\sin\rho\sqrt{2-\sin^2\rho}}{1-\sin^2\rho} \qquad \frac{\sigma'_2}{\sigma'_0} = \left(\frac{1+\sin\rho\sqrt{2-\sin^2\rho}}{1-\sin^2\rho}\right)^2$$

and

$$q_{\max} = p\left(\frac{1+\sin\rho}{1-\sin\rho}\right)\left(\frac{1+\sin\rho\sqrt{2-\sin^2\rho}}{1-\sin^2\rho}\right)^2.$$

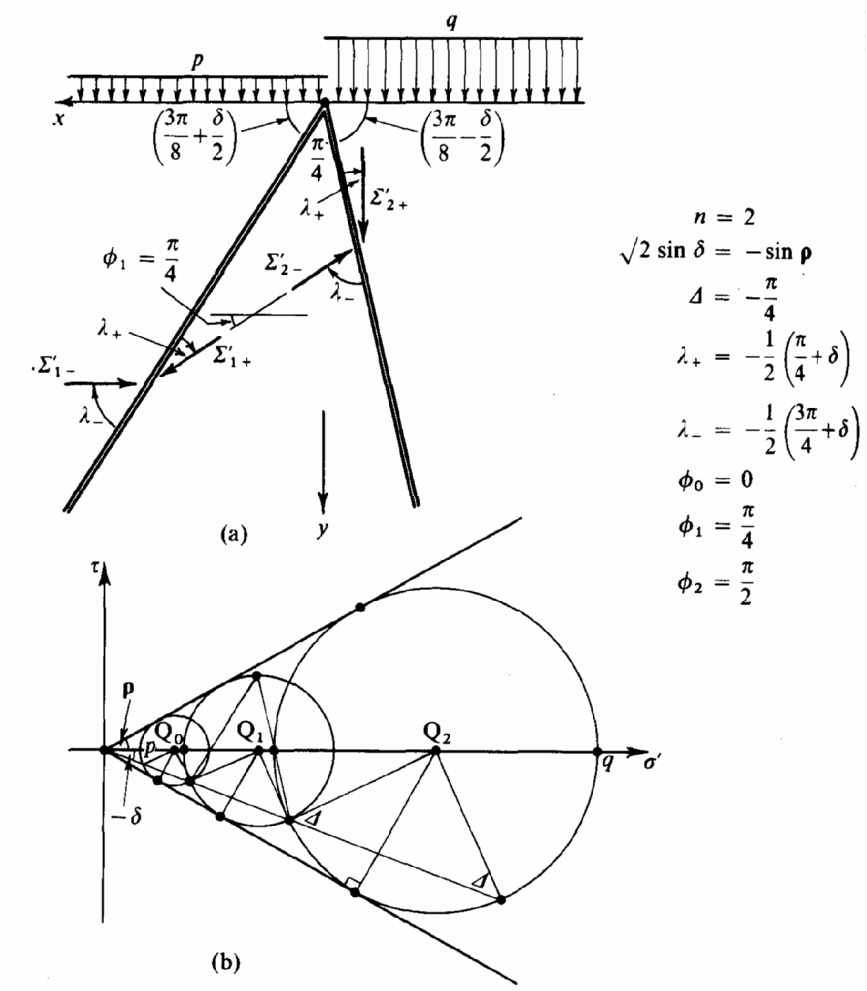

Fig. 9.24 Limiting-stress Field with Two Discontinuities for Frictional Soil

For $\rho = 30^\circ$ this gives $q_{\max} = 14.7p$.

When *n* is *large* we adopt the differential form as before. From eq. (9.16)

$$\sigma'_+ \sin(\Delta - \delta) = \sigma'_- \sin(\Delta + \delta)$$

$$\therefore \quad (\sigma'_+ - \sigma'_-)\sin\Delta\cos\delta = (\sigma'_+ + \sigma'_-)\cos\Delta\sin\delta$$

$$\therefore \quad \frac{(\sigma'_+ - \sigma'_-)}{(\sigma'_+ + \sigma'_-)} = \cot\Delta\tan\delta$$

and as $-\delta \to \rho$

$$\frac{\delta\sigma'}{2\sigma'} = -\cot\left(-\frac{\pi}{2}+\delta\phi\right)\tan\rho = \delta\phi\tan\rho.$$

Integrating, we find that the extreme stress circles are related by

$$\ln\left(\frac{\sigma'_n}{\sigma'_0}\right) = \int_{\sigma'_0}^{\sigma'_n}\frac{d\sigma'}{\sigma'} = \int_0^{\pi/2} 2\tan\rho\, d\phi = \pi\tan\rho$$

which leads to

$$q_{\max} = p\left(\frac{1+\sin\rho}{1-\sin\rho}\right)\exp(\pi\tan\rho).$$

For ρ=30° this gives $q_{\max} \cong 19p$.

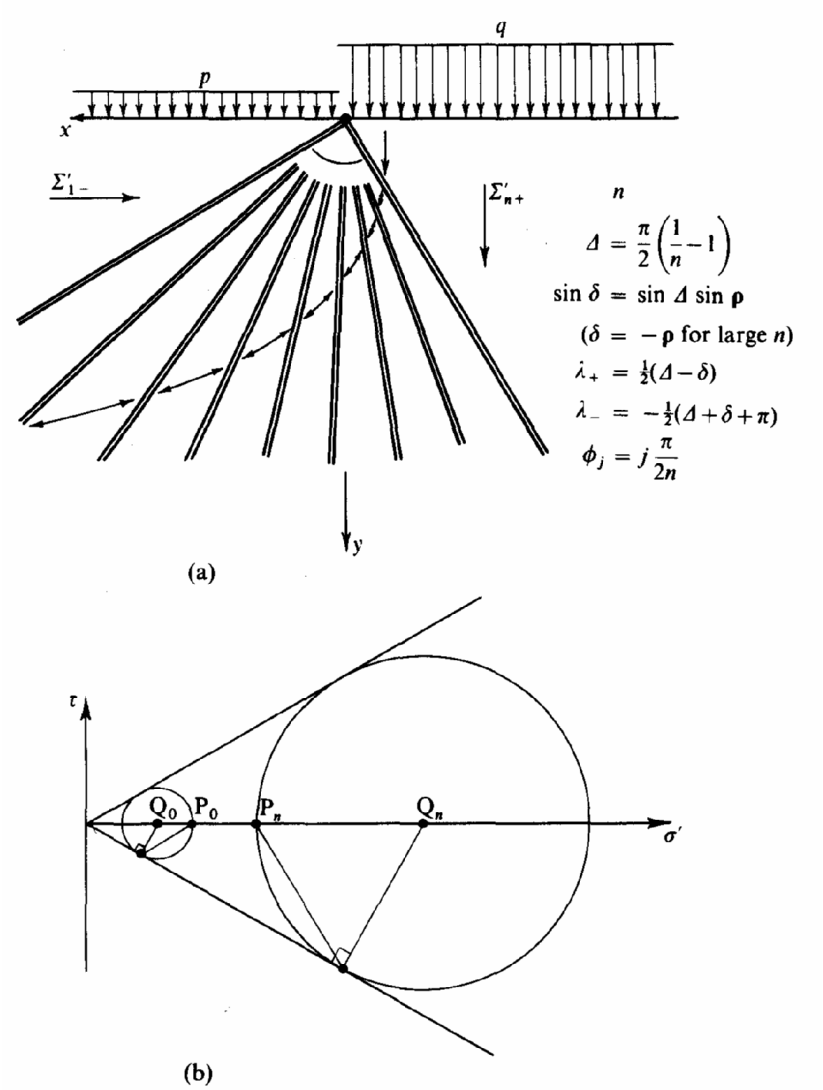

Fig. 9.25 Limiting-stress Field with *n* Discontinuities for Frictional Soil

In the six solutions presented above, each contains regions of *unform* stress separated by strong *discontinuities.* The change of pressure across each discontinuity is characterized by the change of the major principal stress Σ'. Essentially, in this analysis we have replaced the simple idea of one discontinuity of displacement around the surface of a slip circle, by a number of discontinuities of stress which allow successive rotations and changes in magnitude of the major principal stress.

9.7 Upper and Lower Bounds to a Plastic Collapse Load

We now have two strikingly different approximate solutions to the problem of bearing capacity of cohesive ground. In §9.4 our solutions are based on what can be called *kinematically admissible velocity fields*: the mechanism of sliding blocks is compatible with the imposed displacements and the power of the loads moving through the displacements equals the plastic power of dissipation in the cohesive ground. The general solution

$$(q - p) = k\frac{4\alpha}{\sin^2 \alpha} \qquad (9.9 \text{ bis})$$

allows us to take for example in Fig. 9.10

$$\alpha = \frac{\pi}{2} \qquad (q - p) = 2\pi k = \underline{6.28k}$$

or equally to find a minimum at

$$\alpha = 66^\circ\,47' \qquad (q - p) = \underline{5.53k.}$$

In contrast in §9.6 we developed solutions based on what can be called *statically admissible stress fields*: the distributed stresses are in equilibrium with the applied loads and nowhere in the interior do they exceed the yield limit. The distribution with a *single* discontinuity Fig. 9.19 gave us

$$(q - p) = \underline{4k};$$

with *two* discontinuities Fig. 9.20 gave us

$$(q - p) = \underline{4.83k},$$

and a fan of *many* discontinuities Fig. 9.21 gave us

$$(q - p) = \underline{5.14k}.$$

These five estimates of the bearing capacity of cohesive ground can be brought into focus if we take advantage of certain theorems established by Prager and his co-workers.[10] Using some virtual work calculations and the normality condition for perfectly plastic associated flow, they showed that for perfectly plastic material solutions based on kinematically admissible velocity fields must be *upper bounds* to the actual collapse loads, whereas those based on statically admissible stress fields must be *lower bounds*. Hence we estimate that the *actual* bearing capacity $(q - p)_{\max}$ would lie in the range

$$6.28k > 5.53k \geq (q - p)_{\max} \geq 5.14k > 4.8k > 4k.$$

The calculations based on slip circles give us loads that are certainly powerful enough to cause failure in the assumed mechanism, and could well exceed the loads that we would calculate if we were able to think of another more subtle mechanism in which the surface could move down with less power being dissipated in the ground. The calculations based on stress distributions give us loads that the ground could certainly carry in the assumed manner, and these loads could well be exceeded if we were to think of a more subtle distribution by which we could pack a little more stress in the ground. To put the matter even more succinctly, the slip-circle calculations would be all right for demolition experts who wanted to be sure to order enough load to cause a failure; but civil engineers who want to be sure of not overloading the ground ought to think first of stress distributions.

Of course, to say this is to oversimplify the matter. The upper and lower bound theorems are established only for perfectly plastic materials: the present uncertainty about the flow rule and about the instability of soil that comes to fail on the ‘dry side’ of critical states makes it possible only to draw inferences. However, when we recall how slight are the factors of safety commonly used in slope design it is clearly wise to pay close attention to calculations that appear to offer us statically admissible stress distributions. The study of the solutions by the method of characteristics that are set out by Sokolovski becomes particularly attractive.

In the next section we briefly consider the simple effects of bodyweight in horizontal layers of soil of differing properties: in a later section we discuss Sokolovski’s general method for analysis of limiting-stress fields with body-weight acting throughout the field.

9.8 Lateral Pressure of Horizontal Strata with Self Weight ($\gamma > 0, \rho > 0$)

We illustrate the application of Sokolovski's method to the case of Fig. 9.26(a) in which two horizontal layers of frictional soil with different properties are shown to be retained by a smooth vertical wall. (We have chosen a simple problem in order to ease the introduction of further unfamiliar symbols and illustrate the nature of

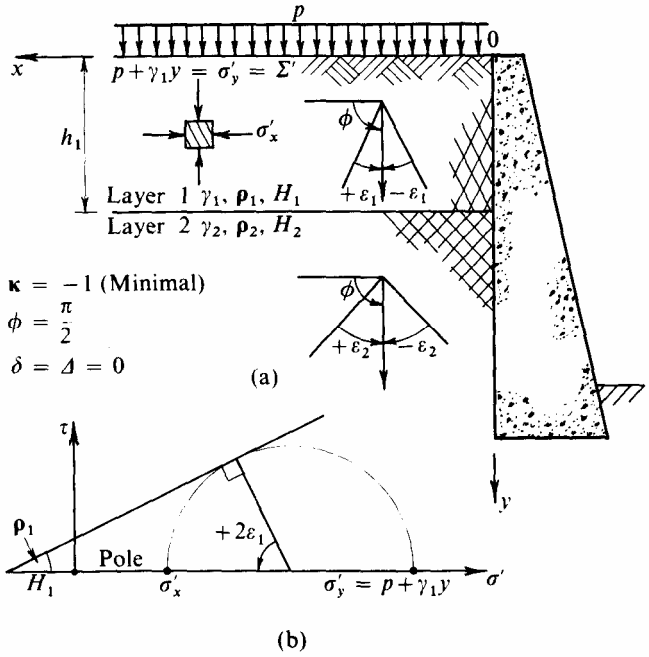

Fig. 9.26 Limiting Lateral Pressure on Retaining Wall: Active Case

Sokolovski's methods; the same solution could be obtained more directly by the conventional method due to Rankine.) The upper layer has thickness h_1 and material properties γ_1, ρ_1 and H_1, while the lower layer has properties γ_2, ρ_2 and H_2 and is of considerable thickness, extending below the base of the wall. A surcharge consisting of a vertical load $p \geq 0$ is assumed to act on the surface; so that Sokolovski's equivalent stress on the surface $(y = 0)$ is simply $p' = p + H_1$.

At a depth y below the surface the vertical stress will be:

$$\left.\begin{aligned} \sigma'_y &= p + \gamma_1 y \qquad (0 \leq y \leq h_1) \\ \sigma'_y &= p + \gamma_1 h_1 + \gamma_2 (y - h_1) \qquad (h_1 \leq y). \end{aligned}\right\} \tag{9.24}$$

In the *minimal* limiting stress state of *active* pressure on the wall the major principal stress Σ' will be vertical $\phi = (\pi/2)$, and the appropriate Mohr's circle for a point at depth y in the upper layer is shown in Fig. 9.26(b).

From the geometry of the figure, the minor principal stress σ'_x is related to σ'_y by the expression

$$\frac{\sigma'_x + H_1}{\sigma'_y + H_1} = \frac{1 - \sin\rho_1}{1 + \sin\rho_1} = \tan^2\left(\frac{\pi}{4} + \frac{\rho_1}{2}\right) = \tan^2 \varepsilon_1 \quad (\rho > 0). \tag{9.25}$$

We have an exactly similar situation for the lower layer, so that we can express the horizontal effective pressure experienced by the retaining wall in the active case as:

$$\left.\begin{aligned} \sigma'_x + H_1 &= (p + \gamma_1 y + H_1)\left(\frac{1-\sin\rho_1}{1+\sin\rho_1}\right) && 0 \le y \le h_1 \\ \sigma'_x + H_2 &= (p + \gamma_1 h_1 + \gamma_2 (y - h_1) + H_2)\left(\frac{1-\sin\rho_2}{1+\sin\rho_2}\right) && h_1 \le y. \end{aligned}\right\} \tag{9.26}$$

The actual *total* pressure on the wall will include the pore-pressure; for fully saturated soil in the absence of any groundwater flow the pore-pressure $u_w = \gamma_w y$ will increase linearly with depth. The values of γ_1 and γ_2 for the soil must take into account any buoyancy effects.

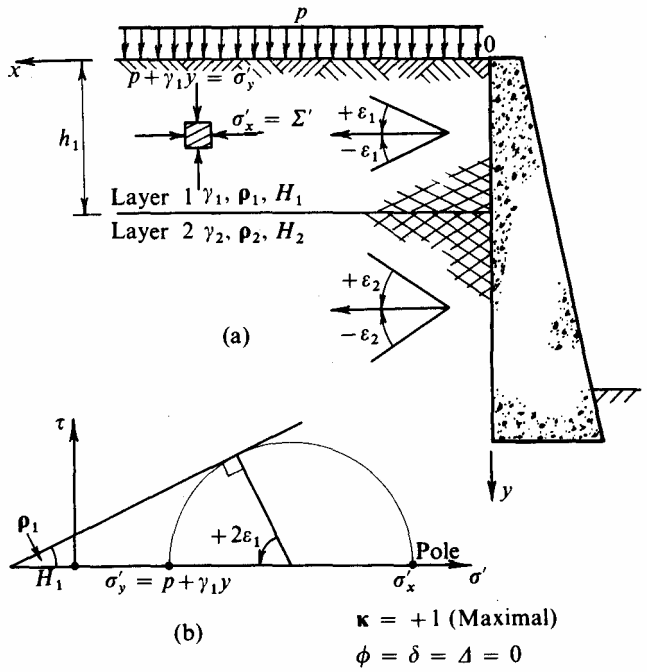

Fig. 9.27 Limiting Lateral Pressure on Retaining Wall: Passive Case

The *passive* case is illustrated in Fig. 9.27(a) where the limiting stress is now *maximal.* The major principal stress is horizontal (ϕ = 0); and in the related Mohr's diagram σ'_x and σ'_y have interchanged their positions from the active case. Equation (9.25) is directly replaced by

$$\frac{\sigma'_y + H_1}{\sigma'_x + H_1} = \frac{1-\sin\rho_1}{1+\sin\rho_1} = \tan^2 \varepsilon_1 \tag{9.27}$$

so that for the *passive* case we have

$$\left.\begin{aligned} \sigma'_x + H_1 &= (p + \gamma_1 y + H_1)\left(\frac{1+\sin\rho_1}{1-\sin\rho_1}\right) && (0 \le y \le h_1) \\ \sigma'_x + H_2 &= (p + \gamma_1 h_1 + \gamma_2 (y - h_1) + H_2)\left(\frac{1+\sin\rho_2}{1-\sin\rho_2}\right) && (h_1 \le y). \end{aligned}\right\} \tag{9.28}$$

Using Sokolovski's elegant notation we can combine eqs. (9.26) and (9.28) and write

$$\left.\begin{aligned} \sigma'_x + H_1 &= (p + \gamma_1 y + H_1)(\tan\varepsilon_1)^{-2\kappa} && (0 \le y \le h_1) \\ \sigma'_x + H_2 &= (p + \gamma_1 h_1 + \gamma_2 (y - h_1) + H_2)(\tan\varepsilon_2)^{-2\kappa} && (h_1 \le y) \end{aligned}\right\} \tag{9.29}$$

where $\kappa = -1$ gives the active case
and $\kappa = +1$ gives the passive case.

In each layer the lateral pressure varies linearly with depth and the distributions are plotted in Fig. 9.28. The slopes

$$\frac{d\sigma'_x}{dy} = \gamma_1 (\tan\varepsilon_1)^{-2\kappa} \qquad (0 \le y \le h_1)$$

$$\frac{d\sigma'_x}{dy} = \gamma_2 (\tan\varepsilon_2)^{-2\kappa} \qquad (h_1 \le y)$$

depend only on the local value of γ and ρ. So change of cohesion ***k*** or surcharge p would only change the datum of the pressure-distribution line (as would a change in pore pressure u_w): it requires a change of density γ or friction ρ to rotate the line.

For the construction of Fig. 9.28 it has been assumed that the groundwater table is at the surface so that the soil is fully saturated, and the submerged bulk densities must be used for calculation of

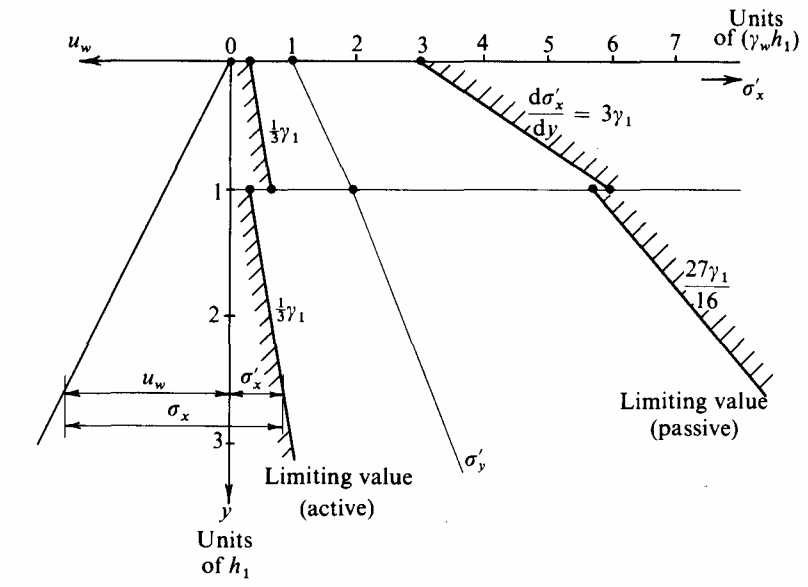

Fig. 9.28 Limiting Lateral Pressure Distribution

effective stresses. The following values have been adopted: $p = \gamma_w h_1$ and for the upper layer

$$\gamma'_1 = \gamma_w, \qquad H_1 = 0, \qquad \tan^2\varepsilon_1 = \tfrac{1}{3}, \qquad i.e., \rho_1 = \pi/6 = 30^\circ$$

and for the lower layer

$$\gamma'_2 = \tfrac{3}{4}\gamma_w, \qquad H_2 = \gamma_w h_1, \qquad \tan^2\varepsilon_2 = \tfrac{4}{9}, \qquad i.e., \rho_2 = 0.3945 = 22^\circ 36'.$$

Across the interface there is, of course, no sudden jump in the value of the vertical effective pressure σ'_y (although its derivative is not continuous); figuratively speaking, if an observer inserted the palm of his hand *horizontally* into the soil he could not detect where the interface was or whether the soil was in a maximal or minimal stress state.

However, just above the interface the lateral effective pressure would be

$$\sigma'_x = (\gamma_w h_1 + \gamma_w h_1 + 0)(3)^{\kappa},$$

i.e., $\sigma'_x = 6\gamma_w h_1$ for $\kappa = +1$, or $\frac{2}{3}\gamma_w h_1$ for $\kappa = -1$

whereas just below

$$\sigma'_x + \gamma_w h_1 = (\gamma_w h_1 + \gamma_w h_1 + \gamma_w h_1)\left(\tfrac{9}{4}\right)^{\kappa},$$

i.e., $\sigma'_x = 5\frac{3}{4}\gamma_w h_1$ for $\kappa = +1$, or $\frac{1}{3}\gamma_w h_1$ for $\kappa = -1$.

An observer who was able to insert the palm of his hand *vertically* could detect the presence of the interface and the state of the soil.

If a greater value of H_2, for example, $H_2 = 2\gamma_w h_1$, had been appropriate, we would have required $\sigma'_x = -\frac{2}{9}\gamma_w h_1$ to bring the soil just below the interface into a minimal limiting state. But since the *effective* stress between the soil and the wall cannot be tensile, Sokolovski introduces the restriction $\sigma'_x \geq 0$ that and concludes that where the mathematical expressions would lead to a negative value of σ'_x the soil cannot be in a limiting state.

In Fig. 9.28 the distribution of pore-pressure u_w has been drawn to the left of the vertical axis of y, with the result that the total lateral pressure at any depth is readily obtained.

Clearly this method can be extended to any number of strata, and can be adapted to take account of other groundwater conditions, or a particular layer that is considered to be purely cohesive.

9.9 The Basic Equations and their Characteristics for a Purely Cohesive Material

In this section we will be covering much of the material set out in Sokolovski's *Statics of Granular Media* §3 and §17, but in detail our treatment will be closer to that presented by Hildebrand.[11]

When we consider the two-dimensional field of stress acting on any material we have two differential equations of equilibrium. For the reference axes of Fig. 9.29 these are:

$$\left.\begin{aligned} \frac{\partial \sigma'_x}{\partial x} + \frac{\partial \tau_{xy}}{\partial y} &= 0 \\ \frac{\partial \tau_{xy}}{\partial x} + \frac{\partial \sigma'_y}{\partial y} &= \gamma \end{aligned}\right\} \tag{9.3}$$

which can be obtained directly by resolving the forces acting on the element, and using the identity of complementary shear stresses ($\tau_{xy} = \tau_{yx}$). We only require one further equation to make the three unknowns $\sigma'_x, \tau_{xy}, \sigma'_y$ determinate.

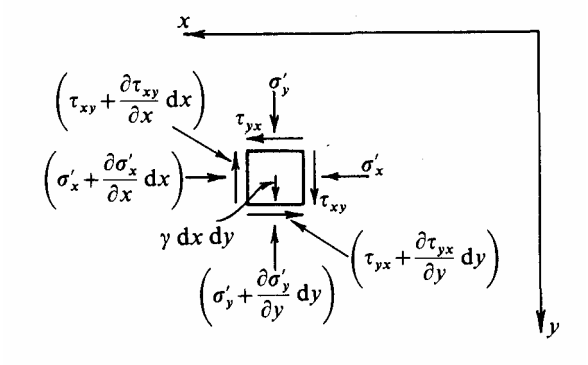

Fig. 9.29 Stresses Acting on Element of Soil

To take a simple example Fig. 9.30(a), consider the calculation of shear stress in a uniform horizontal cantilever of length *l,* of rectangular section with breadth *b* and depth *d,* and carrying a concentrated load *W* at its free end. If we assume the linear distribution of axial stress σ'_x across a vertical section (at a distance *x* from the

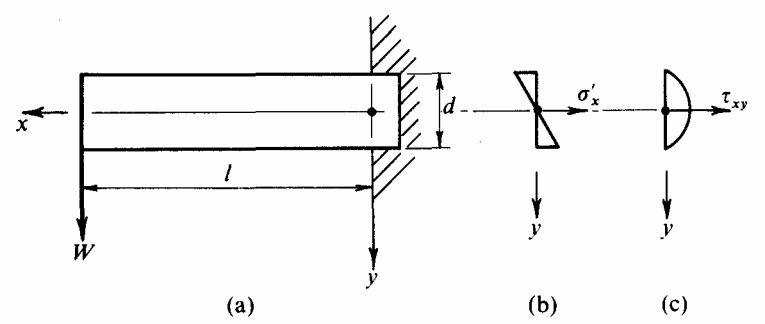

Fig. 9.30 Stress Distributions for Loaded Cantilever

root of the cantilever) in Fig. 9.30(b), then by taking moments we have

$$\frac{\sigma'_x}{y}.\frac{bd^3}{12}=W(l-x). \tag{9.31}$$

This equation is the third one necessary to make the problem completely determinate and we have no further freedom to make other specifications.

The first equilibrium equation (9.30a) gives

$$\frac{\partial\tau_{xy}}{\partial y}=-\frac{\partial\sigma'_x}{\partial x}=+\frac{12W}{bd^3}.y$$

and integrating with the boundary condition $\tau=0$ at $y=\pm d/2$ we obtain the familiar parabolic distribution for shear stress

$$\tau_{xy}=\frac{6W}{bd^3}\left(y^2-\frac{d^2}{4}\right) \tag{9.32}$$

which is illustrated in Fig. 9.30(c). (The second equilibrium equation leads to $\sigma'_y=\gamma y$; in normal circumstances this would be negligible compared with the values of σ'_x and τ_{xy})

It is significant that this result is independent of the actual material of the beam whether it is steel, concrete, wood, or plastic so long as the assumption of the linear distribution of σ'_x remains valid. The material properties will only influence the resulting elastic *strains* of the cantilever.

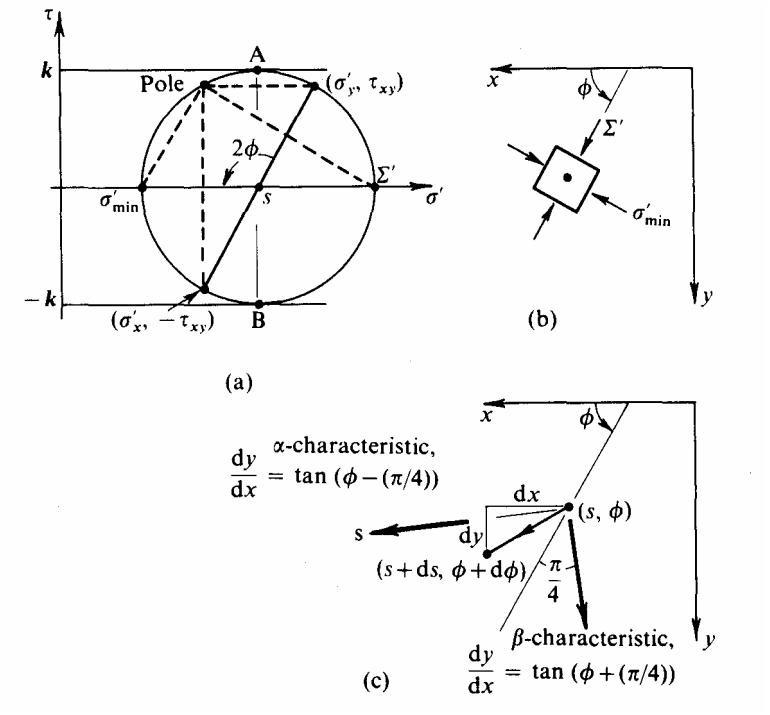

Fig. 9.31 Characteristic Directions for Cohesive Soil

In the same way, in the theory of two-dimensional limiting-stress fields as soon as we postulate that the stresses shall be limiting *everywhere* we have made the problem completely determinate. We now choose to concentrate on purely cohesive materials, so that the condition of limiting stress is given by

$$\tfrac{1}{4}(\sigma'_x - \sigma'_y)^2 + \tau_{xy}^2 = k^2 \tag{9.33}$$

which is the equation to the Mohr's circle of Fig. 9.31.

It is convenient to express this in an alternative form by the parameters s and ϕ (which respectively specify the centre of Mohr's circle and the direction of major principal stress) as follows:

$$\left.\begin{aligned} \sigma'_x &= s + k\cos 2\phi \\ \sigma'_y &= s - k\cos 2\phi \\ \tau_{xy} &= k\sin 2\phi. \end{aligned}\right\} \tag{9.34}$$

Substituting these into the equilibrium eqs. (9.30) we have

$$\left.\begin{aligned} &\frac{\partial s}{\partial x} - 2k\sin 2\phi\frac{\partial \phi}{\partial x} + 2k\cos 2\phi\frac{\partial \phi}{\partial y} = 0 \\ &\frac{\partial s}{\partial y} + 2k\cos 2\phi\frac{\partial \phi}{\partial x} + 2k\sin 2\phi\frac{\partial \phi}{\partial y} = \gamma \\ &\text{which together with the identities for total differentials} \\ &\frac{\partial s}{\partial x}\mathrm{d}x + \frac{\partial s}{\partial y}\mathrm{d}y = \mathrm{d}s \\ &\frac{\partial \phi}{\partial x}\mathrm{d}x + \frac{\partial \phi}{\partial y}\mathrm{d}y = \mathrm{d}\phi \end{aligned}\right\} \tag{9.35}$$

provide four equations for the four unknowns

$$\frac{\partial s}{\partial x}, \frac{\partial s}{\partial y}, \frac{\partial \phi}{\partial x}, \text{and } \frac{\partial \phi}{\partial y}.$$

The solution of the problem of limiting-stress distributions in purely cohesive materials lies in this set of four equations. Leaving aside the special case of finite discontinuity in values of s and ϕ we consider small regions or zones in which there is a continuous variation in values of these parameters. At a typical point (x, y) in Fig. 9.3 1(c) we have data of (s, ϕ) while at an adjacent point $(x + \mathrm{d}x, y + \mathrm{d}y)$ the data are $(s + \mathrm{d}s, \phi + \mathrm{d}\phi)$. If we know values of $\mathrm{d}x$, $\mathrm{d}y$, $\mathrm{d}s$, $\mathrm{d}\phi$ can we find values of $\partial s/\partial x, \partial s/\partial y, \partial \phi/\partial x, \partial \phi/\partial y$, and vice versa? If we can, then a reasonable approximation to the values of s and ϕ in a region surrounding the two points can be obtained by extrapolation. To decide whether this is possible we must examine the equations in detail.

In order to calculate the partial derivatives from given values of $\mathrm{d}x$, $\mathrm{d}y$, $\mathrm{d}s$, and $\mathrm{d}\phi$ we will need to invert the matrix of coefficients on the left-hand side of equations (9.35). This inversion will not be possible when the associated determinant is zero, i.e., when

$$0 = D = \begin{vmatrix} 1 & 0 & -\sin 2\phi & \cos 2\phi \\ 0 & 1 & \cos 2\phi & \sin 2\phi \\ \mathrm{d}x & \mathrm{d}y & 0 & 0 \\ 0 & 0 & \mathrm{d}x & \mathrm{d}y \end{vmatrix} = -(\mathrm{d}y)^2 \cos 2\phi + 2\mathrm{d}x\mathrm{d}y \sin 2\phi - (\mathrm{d}x)^2 \cos 2\phi$$

$$= -\left[\mathrm{d}y - \mathrm{d}x \tan\left(\phi + \frac{\pi}{4}\right)\right]\left[\mathrm{d}y - \mathrm{d}x \tan\left(\phi - \frac{\pi}{4}\right)\right]\cos 2\phi \qquad (9.36)$$

and

$$\tan\left(\phi + \frac{\pi}{4}\right)\tan\left(\phi - \frac{\pi}{4}\right) = 1.$$

Clearly for the directions given by $\mathrm{d}y/\mathrm{d}x = \tan\{\phi \pm (\pi/4)\}$ the determinant is zero; and we shall have no prospect of finding partial derivatives if the values of $\mathrm{d}s$ and $\mathrm{d}\phi$ that are adopted happen to come from adjacent points in one of these *characteristic* directions. It is necessary to study conditions *along* the characteristics.

Sokolovski multiplies the first equation of the set (9.35) by $\sin\{\phi \pm (\pi/4)\}$, the second equation by $-\cos\{\phi \pm (\pi/4)\}$ and adds the results to obtain (after some manipulation)

$$\left[\frac{\partial s}{\partial x} \mp 2k\frac{\partial \phi}{\partial x}\right]\cos\left(\phi \mp \frac{\pi}{4}\right) + \left[\frac{\partial s}{\partial y} \mp 2k\frac{\partial \phi}{\partial y} - \gamma\right]\sin\left(\phi \mp \frac{\pi}{4}\right) = 0. \qquad (9.37)$$

He then introduces two new parameters ξ and η where

$$\left.\begin{aligned} 2k\xi &= s - \gamma y + 2k\phi \\ 2k\eta &= s - \gamma y - 2k\phi. \end{aligned}\right\} \qquad (9.38)$$

Partial differentiation of these parameters and substitution into eq. (9.37) leads to

$$\left.\begin{aligned} \frac{\partial \xi}{\partial x}\cos\left(\phi + \frac{\pi}{4}\right) + \frac{\partial \xi}{\partial y}\sin\left(\phi + \frac{\pi}{4}\right) &= 0 \\ \frac{\partial \eta}{\partial x}\cos\left(\phi - \frac{\pi}{4}\right) + \frac{\partial \eta}{\partial y}\sin\left(\phi - \frac{\pi}{4}\right) &= 0. \end{aligned}\right\} \qquad (9.39)$$

Along the β-characteristic in Fig. 9.31(c),

$$\frac{\mathrm{d}y}{\mathrm{d}x} = \tan\left(\phi + \frac{\pi}{4}\right)$$

we can re-write the first equation as

$$0 = \frac{\partial \xi}{\partial x}\mathrm{d}x + \frac{\partial \xi}{\partial y}\mathrm{d}y = \mathrm{d}\xi \text{ (by definition)}$$

which leads to the important result that

$$\xi = \frac{s - \gamma y}{2k} + \phi = \text{constant} \qquad \left[\frac{\mathrm{d}y}{\mathrm{d}x} = \tan\left(\phi + \frac{\pi}{4}\right)\right]. \tag{9.40}$$

Similarly, *along* the α-characteristic

$$\frac{\mathrm{d}y}{\mathrm{d}x} = \tan\left(\phi - \frac{\pi}{4}\right)$$

the second equation leads to

$$0 = \frac{\partial \eta}{\partial x}\mathrm{d}x + \frac{\partial \eta}{\partial y}\mathrm{d}y = \mathrm{d}\eta,$$

$$\eta = \frac{s - \gamma y}{2k} - \phi = \text{constant} \qquad \left[\frac{\mathrm{d}y}{\mathrm{d}x} = \tan\left(\phi - \frac{\pi}{4}\right)\right]. \tag{9.41}$$

Although we cannot calculate the *partial* derivatives of s and ϕ we do know the *total* differentials of ξ and η along the characteristics. In the next sections we will show how this remarkable property of the characteristics may be used to solve problems of limiting-stress fields in a cohesive soil.

9.10 The General Numerical Solution

We will explain, in general terms, the development of the numerical solution for one simple example that involves a body of purely cohesive soil with self weight, in a *minimal* stress state, below a horizontal boundary Ox on which a vertical surcharge causes an unevenly distributed normal pressure. In Fig. 9.32(a) at points A_{00} and A_{11} on the boundary the normal pressures are p_0 and p_1, where

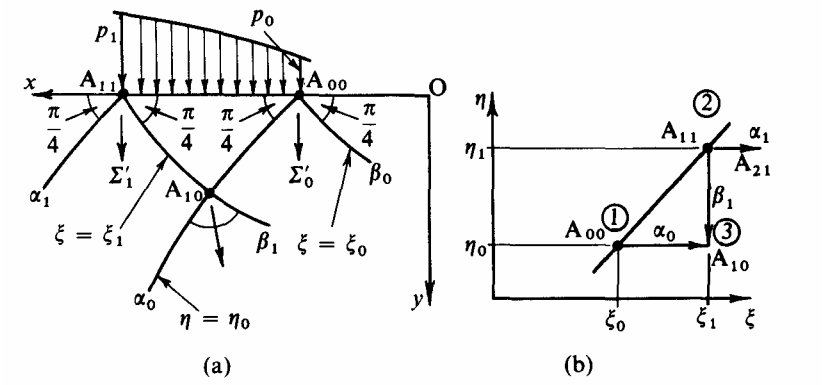

Fig. 9.32 Mapping of Characteristics for Numerical Solution

$p_0 < p_1$. Just below each of these points the states of stress in the soil are defined by

$$\left.\begin{aligned} s_0 &= p_0 - k \qquad \phi_0 = \frac{\pi}{2}, \\ s_1 &= p_1 - k \qquad \phi_1 = \frac{\pi}{2}. \end{aligned}\right\} \tag{9.42}$$

From these values we calculate

$$\xi_0 = \frac{p_0}{2k} - \frac{1}{2} + \frac{\pi}{2} \qquad \eta_0 = \frac{p_0}{2k} - \frac{1}{2} - \frac{\pi}{2}$$
$$\xi_1 = \frac{p_1}{2k} - \frac{1}{2} + \frac{\pi}{2} \qquad \eta_1 = \frac{p_1}{2k} - \frac{1}{2} - \frac{\pi}{2}$$

in Fig. 9.32(b) we display the plane of characteristics (ξ, η) on which we can plot points A_{00} and A_{11}.

Through A_{00} we draw the characteristic $\eta = \text{const.} = \eta_0$, through A_{11} we draw the characteristic $\xi = \text{const.} = \xi_1$, and these intersect in the point A_{10}. The point A_{10} is such that and therefore

$$\left.\begin{aligned} \xi &= \frac{s}{2k} + \phi - \frac{\gamma y}{2k} = \xi_1 = \frac{p_1}{2k} - \frac{1}{2} + \frac{\pi}{2} \\ \eta &= \frac{s}{2k} - \phi - \frac{\gamma y}{2k} = \eta_0 = \frac{p_0}{2k} - \frac{1}{2} - \frac{\pi}{2} \end{aligned}\right\} \tag{9.43}$$

and the stress parameters s and ϕ at the point A_{10} are clearly

$$\left.\begin{aligned} s &= \frac{p_1 + p_0}{2} - k + \gamma y \\ \phi &= \frac{p_1 - p_0}{4k} + \frac{\pi}{2}. \end{aligned}\right\} \tag{9.44}$$

So the consequence of the property of the characteristics (that total differentials are known along them) is that we now know exactly what the stresses are at this point A_{10} in the soil below the loaded surface. The remaining numerical problem is simply one of mapping; to find where the point A_{10} is on the (x, y) plane — that is to map the sheet $A_{11}A_{10}A_{00}$ from the (ξ, η) plane on to the (x, y) plane.

Sokolovski gives an approximate method that is quite effective for mapping out these points. A table is drawn up where each row and each column correspond to a characteristic. The table resembles the construction of lines on the (ξ,η) plane in Fig. 9.32(b). Diagonally across the table the values given to parameters (x, y, s,ϕ) are those for the appropriate positions on the boundary. At two points 1 and 2 within the table let the values (x_1, y_1, s_1,ϕ_1) and (x_2, y_2, s_2,ϕ_2) be known. To find the values at the next successive point 3, replace the differential equations by *recurrence formulae*

$$\left.\begin{aligned} &\left.\begin{aligned} (y_3 - y_1) &= (x_3 - x_1)\tan\left(\phi_1 - \frac{\pi}{4}\right) \\ s_3 - s_1 - 2k(\phi_3 - \phi_1) &= \gamma(y_3 - y_1) \end{aligned}\right\} \eta = \text{const.} \\ &\left.\begin{aligned} (y_3 - y_2) &= (x_3 - x_2)\tan\left(\phi_2 + \frac{\pi}{4}\right) \\ s_3 - s_2 - 2k(\phi_3 - \phi_2) &= \gamma(y_3 - y2) \end{aligned}\right\} \xi = \text{const.} \end{aligned}\right\} \tag{9.45}$$

and hence the values of (x_3, y_3, s_3,ϕ_3) may be determined. As this programme of calculation is followed so successive compartments of the table are filled. The numbers in each compartment fix the position of one node in the pattern of characteristics shown in Fig. 9.32(a) and the state of stress at that node.

It is clear that although the above paragraphs only cover one example, the same method will apply to soil with internal friction, with or without self weight: of course different recurrence formulae will be appropriate for different problems[12] and special

formulae will have to be developed to meet special difficulties at some boundaries, but for all such developments direct reference should be made to Sokolovski's texts.

9.11 Sokolovski's Shapes for Limiting Slope of a Cohesive Soil

We now consider Sokolovski's use of integrals of the equations of limiting equilibrium in regions throughout which either ξ or η has constant values. We consider only regions where ξ is constant, since those with η constant are the exact converse and the families of characteristics become interchanged. In the regions where ξ is constant everywhere and η varies then

$$\frac{s-\gamma y}{2k}+\phi=\xi=\xi_0=\text{constant} \tag{9.46}$$

and the one constant ξ_0 applies to *every* β-characteristic. The family of α-characteristics for which $\mathrm{d}y=\mathrm{d}x\tan(\phi-\pi/4)$ must become a set of straight lines since

$$\eta=\frac{s-\gamma y}{2k}-\phi=\xi-2\phi=\xi_0-2\phi \tag{9.47}$$

so that $\mathrm{d}\eta=-2\mathrm{d}\phi$ and ϕ will be constant along each α-characteristic. The equation of any α-characteristic becomes

$$\frac{y-y(\phi)}{x-x(\phi)}=\tan\left(\phi-\frac{\pi}{4}\right) \tag{9.48}$$

where $(x(\phi), y(\phi))$ are the coordinates of some fixed point on the characteristic.

For the special case when all α-characteristics pass through one point we can choose it as the origin of coordinates so that $x(\phi)\equiv y(\phi)\equiv 0;$ and the family of α-characteristics is simply a fan of radial straight lines. The curved β-characteristics having

$$\mathrm{d}y=\mathrm{d}x\tan\left(\phi+\frac{\pi}{4}\right)$$

are then segments of concentric circles orthogonal to these radii.

Solutions to specific problems can be constructed from patchwork patterns of such regions, as we see for the general case of the limiting stability of a slope of a cohesive soil shown in Fig. 9.34 (and as we saw for the case of high-speed fluid flow in Fig. 1.8). The essential feature of these solutions is that the values of one parameter (ξ in Fig. 9.34) which are imposed at one boundary (OA_0) remain unchanged and are propagated through the pattern and have *known* values at a boundary of interest ($0A_3$).

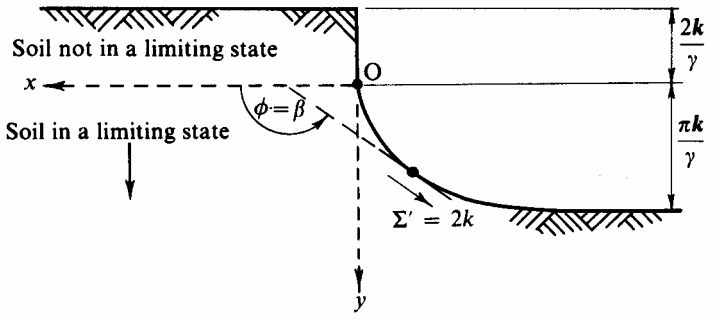

Fig. 9.33 Limiting Shape of Slope in Cohesive Soil

A limiting shape for a slope in cohesive soil is shown in Fig. 9.33 and we begin by making

a simple analysis of conditions along the slope, which forms the boundary of interest. Above O there is a vertical face of height $h = 2k/\gamma$ for which the soil (of self-weight γ and cohesion k) is *not* in a limiting state. At any point on the curved slope the major principal stress is at an angle ϕ equal to the angle β of the slope at that point, and of magnitude $2k$ so that the values of the parameters s and ϕ along the curve are

$$s = k \quad \text{and} \quad \phi = \beta \tag{9.49}$$

In Fig. 9.33 we have taken the slope at O to be vertical so that $\beta = \beta_0 = \pi/2$, but in Fig. 9.34 we show a generalized slope problem where the weight of soil above the line OA_0 is replaced by a uniformly distributed surcharge p, and $\beta_0 \neq \pi/2$. Below the line OA_0 in Fig. 9.34 is a region A_0OA_1 dependent on the conditions along the boundary OA_0. It is a region of a single state (ξ_0, η_0) with straight parallel characteristics in each direction and with

$$\left.\begin{aligned} s &= p + \gamma y - k \qquad \phi = \pi/2 \\ \xi &= \xi_0 = \frac{p-k}{2k} + \frac{\pi}{2} \\ \eta &= \eta_0 = \frac{p-k}{2k} - \frac{\pi}{2} \end{aligned}\right\} \tag{9.50}$$

The shape of the slope must be such that retains the value given in eq. (9.50), and that the conditions of eq. (9.49) are satisfied.

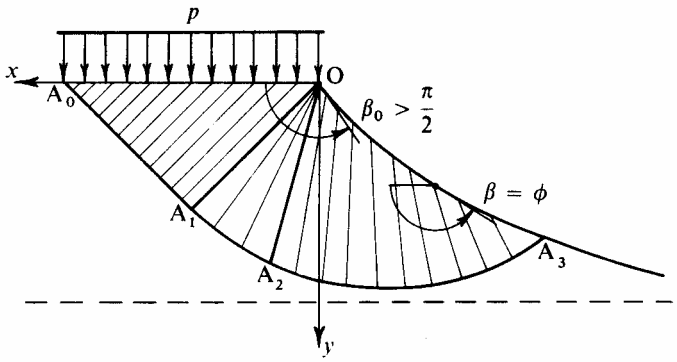

Fig. 9.34 General Limiting Shape of Slope in Cohesive Soil (After Sokolovski)

We have, therefore,

$$\xi = \frac{s - \gamma y}{2k} + \phi = \frac{k - \gamma y}{2k} + \beta \quad \text{and} \quad \xi = \xi_0 = \frac{p-k}{2k} + \frac{\pi}{2},$$
$$\text{so that} \qquad y = \frac{2k}{\gamma}(\beta - \beta_0) \qquad \text{where } \beta_0 = \left(\frac{p}{2k} + \frac{\pi}{2} - 1\right). \tag{9.51}$$

But at any point on the slope $\mathrm{d}y = \mathrm{d}x \tan\beta$ so that substituting for y from eq. (9.51) we find

$$\mathrm{d}x = \frac{2k}{\gamma}\cot\beta\,\mathrm{d}\beta$$

which can be integrated to give

$$\frac{\gamma x}{2k} = \ln\left(\frac{\sin\beta}{\sin\beta_0}\right). \tag{9.52}$$

The limiting slope must therefore have as its equation

$$\frac{\gamma x}{2k} = \ln \frac{\sin(\beta_0 + \gamma y/2k)}{\sin \beta_0} \tag{9.53}$$

and have a horizontal asymptote

$$\frac{\gamma y}{2k} = \pi - \beta_0 \tag{9.54}$$

Various slope profiles corresponding to different values of β_0 are shown in Fig. 9.35 which is taken from Fig. 178 of the earlier translation of Sokolovski's text.

In the particular case of Fig. 9.33 when $\beta_0 = \pi/2$ the slope equation becomes

$$\frac{\gamma x}{2k} = \ln \cos\left(\frac{\gamma y}{2k}\right) \tag{9.55}$$

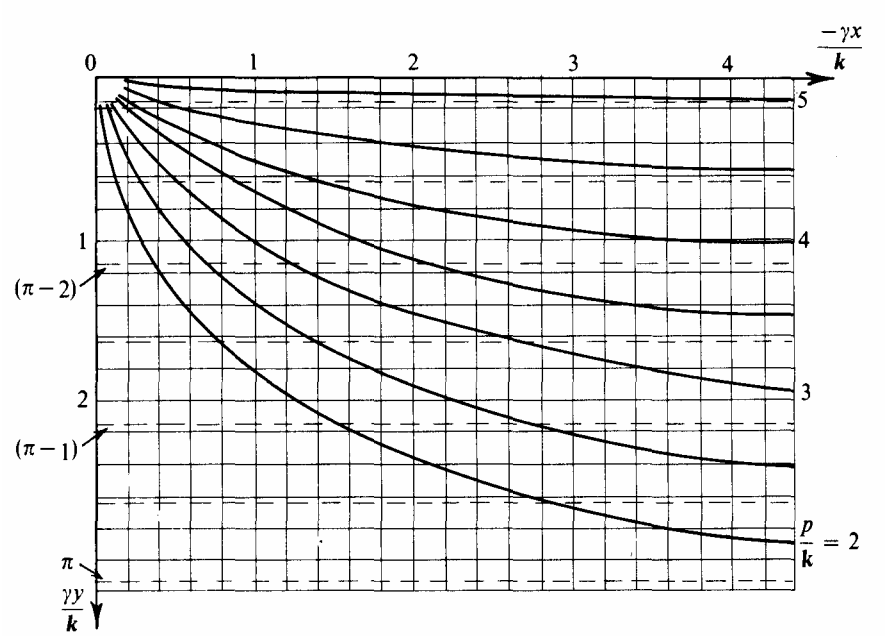

Fig. 9.35 Limiting Shapes of Slope in Cohesive Soil for Various Values of Surcharge (After Sokolovski)

having a horizontal asymptote $y = \pi k/\gamma$. Thus the maximum difference in height between the left and right hand levels of Fig. 9.33 is $(2+\pi)k/\gamma$, which is the maximum difference predicted in §9.7.

9.12 Summary

At this stage of the book we are aware of the consequences of our original decision to set the new critical state concept among the classical calculations of soil mechanics. Our new models allow the prediction of *kinematics* of soil bodies, and yet here we have restricted our attention to the calculation of limiting equilibrium and have introduced Sokolovski's classical exposition of the *statics* of soil media. The reason for this decision is that it is this type of statical calculation that at present concerns practical engineers, and the capability of the new critical state concept to offer rational predictions of *strength* is of immediate practical importance. In this chapter we have reviewed the manner of working of the classical calculations in which the only property that is attributed to soil is strength. We hope that this will give many engineers an immediate incentive to make use of the new

critical state concept, and perhaps in due course become actively interested in the development of new calculations of *deformation* that the concept should make possible.

References to Chapter 9

1 Coulomb, C. A. Essai sur une application des règles de maximis et minimis a quelques problémes de statique, relatifs a l'architecture, *Mémoires de Mathématique de l'Académie Royale des Sciences,* Paris, 7, 343 – 82, 1776.

2 Terzaghi, K. Large Retaining Wall Tests, *Engineering News Record,* pp. 136, *259,* 316, 403, 503, 1934.

3 Coulomb, C. A. Théorie des machines simples, *Mémoires de Mathématique de l'Académie Royale des Sciences,* Paris, 10, 161 – 332, 1785.

4 Petterson, K. E. The Early History of Circular Sliding Surfaces, *Géotechnique,* 5, *275 –96,* 1955.

5 Fellenius, W. *Erdstatische Berechnungen,* Ernst, Berlin, 1948.

6 Taylor, D. W. *Fundamentals of Soil Mechanics,* Wiley, 1948.

7 Janbu, N. Earth Pressures and Bearing Capacity Calculations by Generalised Procedure of Slices, *Proc. 4th mt. Conf Soil Mech. and Found. Eng.,* London, vol 2, pp. 207 – 12, 1957.

8 Bishop, A. W. and Morgenstern, N. R. Stability Coefficients for Earth Slopes, *Géotechnique,* 10, 129 – 50, 1960.

9 Sokolovski, 'V. V. *Statics of Granular Media,* Pergamon, 1965.

10 Prager, W. *An Introduction to Plasticity,* Addison-Wesley, 1959.

11 Hildebrand, F. B. *Advanced Calculus for Application,* Prentice-Hall, 1963.

12 Mukhin, I. S. and Sragovich, A. I. Shape of the Contours of Uniformly Stable Slopes, *Inzhenernyi Sbornik,* 23, 121 – 31, 1956.